U.PORTO
INSTITUTO DE CIÊNCIAS BIOMÉDICAS ABEL SALAZAR
UNIVERSIDADE DO PORTO

U.PORTO
FEUP FACULDADE DE ENGENHARIA
UNIVERSIDADE DO PORTO

The Structure and Plasticity of the Proximal Axon of Hippocampal and Dorsal Root Ganglion Neurons

Ana Isabel Delgado Cravo Lopes Nascimento

Master Dissertation – Temporary Version

Integrated Master in Bioengineering – Branch of Molecular Biotechnology

Supervisor: Dr. Fernando Mar

Co-supervisor: Dr. Mónica Sousa

Instituto de Biologia Molecular e Celular (IBMC)

Instituto de Investigação e Inovação em Saúde (I3S)

University of Porto

September 2016

“The mystery of human existence lies not in just staying alive, but in finding something to live for.”

Fyodor Dostoyevsky

Agradecimentos

Esta tese, tal como toda a minha vida académica, só se concretizou devido à ajuda de pessoas incríveis que tive a sorte de encontrar pelo caminho.

Quero agradecer ao Fernando, por tudo o que me ensinou e pelo acompanhamento próximo, paciente e generoso.

Agradeço também à Mónica, por ser uma cientista tão inspiradora e cuja assertividade, rigor e simplicidade foram essenciais para este trabalho.

Aos elementos do grupo Nerve Regeneration, por estarem sempre disponíveis e por criarem um ambiente peculiar onde é bom trabalhar.

Ao Pedro Óscar e à Ana Luísa, pelo carinho de longa data do qual não prescindo.

À minha mãe e ao meu pai, por serem as minhas principais referências, pela sua força, honestidade pessoal e excelência profissional. Sou uma sortuda por serem meus pais.

Mãe, agradeço-te a garra desmesurada e o carinho com que me acompanhaste sempre. Agradeço-te também a dedicação, iterada milhares de vezes em rotinas diárias, graças à qual consigo respirar. Obrigada por tudo.

Table of Contents

List of Abbreviations

AIS	Axon Initial Segment
AnkG	Ankyrin-G
CAM	cell adhesion molecule
CHX	cycloheximide
CNS	central nervous system
DIV	days *in vitro*
DRG	dorsal root ganglion
E	embryonic days
ER	endoplasmic reticulum
EtOH	ethanol
FBS	fetal bovine serum
GFP	green fluorescent protein
HBSS	Hanks' Balanced Salt solution
HEBS	HEPES-buffered saline
KCl	potassium chloride
Kv	voltage-gated potassium
NaCl	sodium chloride
Nav	voltage-gated sodium
NF	186-kDa Neurofascin
NIRB	near-infrared branding
P	postnatal day
P/S	penicillin–streptomycin
PS	proximal segment
PBS	phosphate-buffered saline
PFA	paraformaldehyde
SGC	satellite glial cell
shRNA	short hairpin RNA

YFP	yellow fluorescent protein

List of Figures

List of Tables

Abstract

The Axon Initial Segment (AIS) of multipolar neurons is a key specialized region of utmost importance for neuronal physiology as it maintains axonal identity and generates action potentials. The AIS is regarded as a highly stable structure comprised by remarkably long-lived molecules, with the exception of Ankyrin-G (AnkG). However, multipolar neurons regulate their intrinsic excitability via plastic changes in AIS length and location. Notably, understanding how the AIS plasticity is regulated may help understand its importance in neuro-pathologies like epilepsy, bipolar disease, and intellectual disability.

Here we investigated the mechanism of AIS relocation in response to chronic depolarization in dissociated hippocampal neurons. Using cycloheximide, a protein synthesis inhibitor, we showed that protein synthesis is needed for the maintenance and relocation of the AIS. Using a more specific approach, we demonstrated that two AIS molecules, Neurofascin and βIV-Spectrin, are short-lived at the AIS and their synthesis is needed for both AIS maintenance and relocation. Furthermore, the removal of βIV-Spectrin led to a complete disassembly of the AIS, suggesting that AnkG is not the only essential component required for AIS maintenance. In summary, our results challenge the current paradigm that AIS molecules are long-lived and AnkG is the only essential component necessary for AIS maintenance.

In contrast with multipolar neurons, pseudo-unipolar neurons possess a remarkably unique morphology since they have one axon emerging from the cell body (stem process) which forms a T-junction originating two axons. An important example of pseudo-unipolar neuron is the dorsal root ganglion (DRG) neuron, which has been extensively studied because of its key role in the transmission of sensory signals. It has been suggested that the stem process has a region with a molecular composition similar to the AIS named proximal segment (PS). So far, many basic questions remain unanswered regarding the fine structure and physiology of DRG neurons. It is not known what ultrastructural differences justify the strikingly different functional properties of central and peripheral axons and whether the PS contribute to such features.

In this work we aimed at understanding the contribution of the PS for DRG neuron morphology and central-peripheral asymmetry. Since there are no *in vitro* models described in the

literature for DRG neurons with pseudo-unipolar morphology containing PS, we successfully developed this model using long-term primary co-cultures of embryonic rats. In addition, we showed *in vitro* that contact with non-neuronal cells is necessary for pseudo-unipolarization and PS formation. The definite ultrastructure of the stem process and axonal branches has never been described. By using a correlative light and electron microscopy methodology, we aim at determining *in vivo* the ultrastructure of those regions. We were able to establish this technique, with the ultrastructural analysis being underway.

Overall, we have worked on two exciting frontiers of neuroscience. We have expanded the knowledge on AIS plasticity and we developed an *in vitro* model for pseudo-unipolar DRG neurons. Also, the analysis of the ultrastructure of DRG neurons is being performed.

CHAPTER 1

Introduction

I. The Multipolar Morphology and the Axon Initial Segment

1. Neuronal Structure

1.1. Morphological classification of neurons

Based on morphological characteristics, most common vertebrate neurons are classified into the following classes: multipolar, bipolar, and pseudo-unipolar (fig. 1). Multipolar neurons (fig. 1A) are the most common type in vertebrates and make up virtually all of the neurons of the central nervous system (CNS), for instance cortical and hippocampal neurons. They possess several dendrites and one long axon projecting from the soma. In contrast, bipolar neurons (fig. 1B), which are sensory neurons (for instance retinal bipolar cells), have two processes arising from the cell body, one on each end. The dendrites, which are located in the end of one process, receive sensory information, which is then transmitted to the CNS via the axon on the other end. Concerning pseudo-unipolar neurons (fig. 1C), a single process arises from the soma and divides into two branches, with one branch projecting to the periphery and the other projecting to the CNS. Sensory information collected by the peripheral branch is transmitted to the CNS via the other branch. Examples of this type of cell are sensory cells in the DRG [1].

1.2. Neuronal subcellular domains

Multipolar neurons possess basic morphological components: the cell body, the dendrites, and the axon (fig. 2).

The cell body, also called soma, contains a single nucleus surrounded by a large number of organelles responsible for the metabolic requirements of the cell [2].

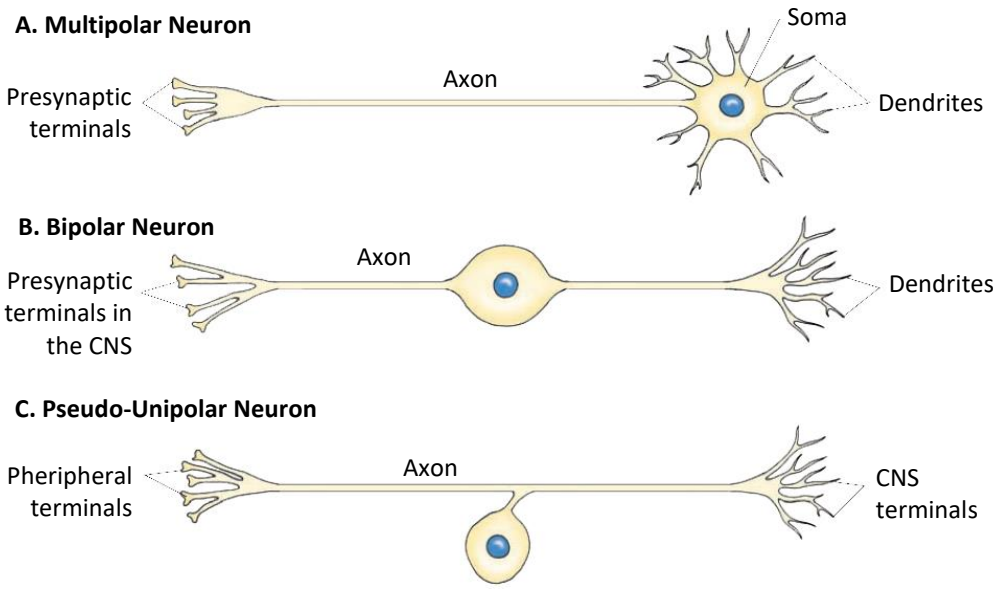

Fig. 1. Most common neuronal types in vertebrates: multipolar (A), bipolar (B), and pseudo-unipolar (C) neurons. Adapted from [1].

Dendrites are one of two types of neuronal processes which emerge from the soma. Dendrites receive chemical signals from other neurons through neurotransmitter receptors. In response to afferent information, they integrate the synaptic inputs and generate electrical signals. As far as morphology is concerned, there are generally between one and nine dendrites arising from the soma, and in some neuronal populations each dendrite may branch many times, giving a complex treelike structure known as dendritic tree. Dendrites are relatively short and thick, but become thinner with increased distance from the soma. In addition, they present an irregular outline due to the presence of numerous protusions such as dendritic spines [3]. Regarding ultrastructural features, dendrites possess both rough and smooth endoplasmic reticulum (ER) active in protein synthesis, as well as Golgi-like structures known as Golgi outposts. Importantly, dendrites possess the requisite cellular machinery for local trafficking of lipids and membrane proteins through the canonical secretory pathway [4].

The axon is the other type of neuronal process emerging from the soma. Overall, axons are responsible for the transmission of information once an action potential is generated [5]. The region of the soma from which an axon originates is called the axon hillock. At the beginning of the axon, there is an important specialized region, known as the AIS, which will be discussed in detail later on. Generally, a single axon emerges from the cell body. Axonal morphology is highly variable: axon diameter and extent vary considerably between neuronal populations, and axons

may branch, originating axonal arborization with variable complexity. In contrast to dendrites, the axon has an uniform diameter along its entire extent, and axons and its collaterals may be surrounded by myelin sheath [3]. In some neurons, axons present numerous varicosities along them, which constitute synaptic contacts with target cells and are known as 'boutons en passant'. Each axon terminates with multiple branches known as telodendria. This structure contains the presynaptic terminals, which can also be called terminal boutons [5]. Regarding ultrastructural features, axons present a peculiar organelle distribution. Only smooth ER-like structures have been detected in axons, and no Golgi or rough ER have been reported, which makes the secretory mechanism not clear [6]. Several reports identified ribosomes in vertebrate axons, which is an evidence for local protein synthesis in axons [7].

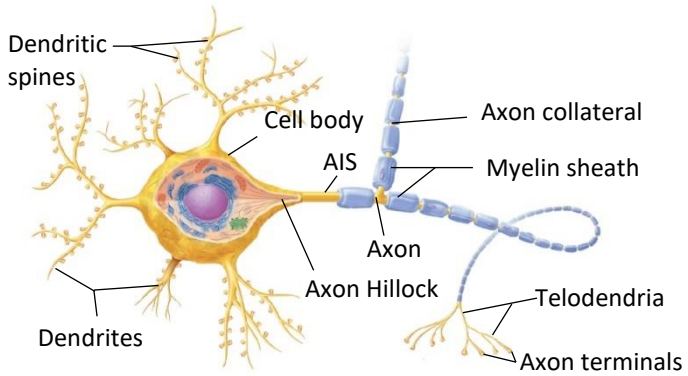

Fig. 2. Structure of multipolar neurons. Adapted from [8].

2. Molecular Insights of Neuronal Polarity

Multipolar neurons are one of the most polarized cell types due to the asymmetry of axons and dendrites, which constitute two molecularly and functionally distinct compartments [9].

Neuronal polarization can be divided into specific steps. *In vivo*, mammalian neurons usually migrate to their final destination upon cell cycle exit. During migration, neurons form a leading process and a trailing process, each becoming the axon or dendrites depending on the cell type [9].

During the last 15 years enormous advances have been made in the understanding of the basic molecular machinery involved in the development of neuronal polarity [10]. Many factors have emerged as crucial players in the development of neuronal polarity, including regulators of microtubule and actin dynamics and molecular motors that show axon-dendrite selectivity [11].

The cell-autonomous establishment of neuronal polarity has been studied mainly in primary cultures of dissociated rodent embryonic hippocampal neurons and postnatal cerebellar granule neurons [11]. In dissociated cultures, hippocampal neurons display specific transitions (fig. 3). First, neuritogenesis occurs: neurons establish several, apparently identical, immature neurites (stage 2). Then, axonogenesis takes place: a single neurite grows rapidly to become the axon, while the other neurites only later develop into dendrites (stage 3). Finally, rapid axon and dendritic outgrowth occurs (stage 4), followed by terminal neuronal differentiation (stage 5) [12].

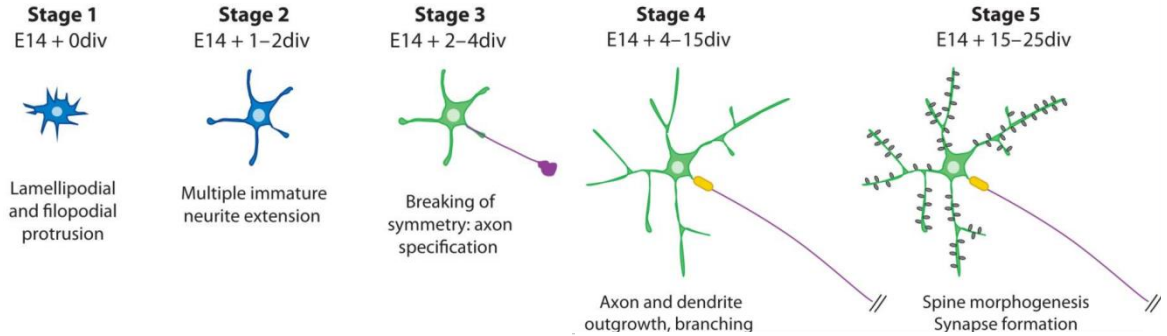

Fig. 3. Specific transitions of polarization of postmitotic hippocampal neurons *in vitro*, as classically described by [12]. Image from [9].

3. The Axon Initial Segment

Central to the neuronal polarity of multipolar neurons is the AIS. The AIS is a specialized ~20–40-µm-long structure located in the proximal axon [13]. Therefore, the AIS physically separates the somadendritic compartment from the axon. This segment is also a physiological bridge, since it serves crucial functions: conversion of somatodendritic inputs into all-or-none action potentials, control of neuronal excitability and maintenance of neuronal polarity [14].

Interestingly, AIS assembly is an intrinsic property of neurons, since no extracellular cues are required [15]. In dissociated cultured neurons, after the axon starts to grow, initial segment components become increasingly enriched at the AIS, with a large majority of cells showing a 'mature' AIS by 7 days *in vitro* [13, 16].

3.1. Molecular organization of the AIS

The consensus in the field is that the defining molecular component of the AIS is the cytoskeletal protein AnkG [17], because loss of AnkG not only prevents AIS molecular assembly but also promotes its disassembly [18, 19]. Recently, it was shown that AnkG assembles by exclusion and not by recruitment. The distal actin subcortical cytoskeleton of the axon is progressively filled with Ankyrin-B from its distal end towards the cell body, and leaves the remaining proximal axon free for AnkG assembly [20]. Nevertheless, it is still unknown how this intra-axonal boundary is reproducibly established.

D'Este *et al*. (2015) used unprecedented imaging capabilities to study the actin cytoskeleton of cultured hippocampal neurons. They showed that subcortical actin is organized in regularly spaced rings encompassing the shaft along the length of both axons and dendrites [21]. These ring-like structures are formed by short actin-filaments that are connected by Spectrin tetramers that create a uniform spacing of ~180–190 nm between rings [22]. More recently, Leterrier *et al.* (2015) determined the AIS nanoscale architecture with super-resolution microscopy (fig. 4) [23]. In the AIS, actin rings are connected by longitudinal head-to-head βIV-Spectrin subunits. βIV-Spectrin is a scaffolding protein specifically located in the AIS [22, 23]. It has been suggested that AnkG is not the only component which is essential for the organization of the AIS, since βIV-Spectrin deletion leads to alterations in the organization of such structure [24, 25]. AnkG binds simultaneously to βIV-Spectrin subunits and to several membrane-associated proteins, so it binds AIS components to the subcortical actin cytoskeleton [23]. Of interest, there are also long longitudinal actin bundles along the AIS [26].

Microtubules form dense parallel arrays (bundles) in axons and dendrites. Axonal microtubules have uniform orientation, with their plus ends facing the axon tip [10]. A distinct feature of the AIS structure is the presence of microtubule fascicles, which are groups of closely spaced microtubules linked by thin cross bridges [27]. These microtubules localize more deeply within the AIS cytoplasm and are linked to AnkG by end binding proteins [28].

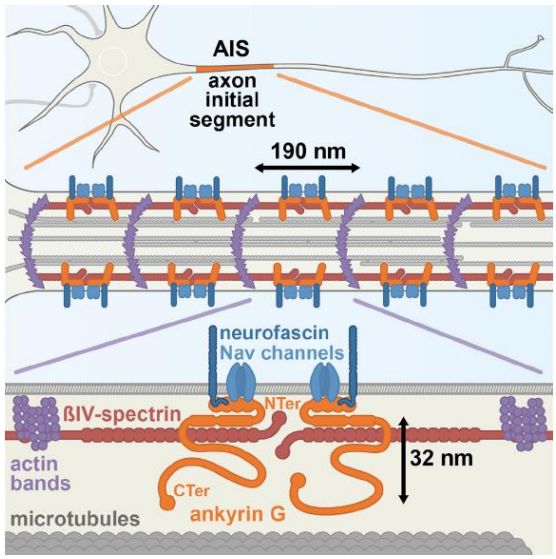

Fig. 4. The AIS nanoscale architecture as revealed by super-resolution microscopy. Image from [23].

A variety of voltage-gated Na^+, K^+, and Ca^{2+} channels are enriched at the AIS. The high concentration of voltage-gated sodium (Nav) channels at the AIS contributes for making it the lowest threshold site for action potential initiation [29]. Different types of neurons or even the same neuron at different developmental stages possess distinct subtypes of ion channels, and there is also variability in their distribution along the AIS [30]. Importantly, the arrangement of ion channels at the AIS determine the action potential generation, pattern, and shape [31]. Moreover, all Nav channels and also a subset of voltage-gated potassium (Kv) channels possess a motif that is essential for binding to AnkG and consequently determine their accumulation at the AIS [32]. In contrast, a different subset of Kv channels (Kv_1) is clustered by the scaffolding protein PSD-93, and finally the molecular mechanisms regulating Ca^{2+} channels are unknown [30].

The AIS is also enriched in cell adhesion molecules (CAMs). CAMs of the L1 family, namely 186-kDa Neurofascin (NF) and neuron glia-related CAM, bind to AnkG. In contrast, the other CAMs also present in this segment (TAG-1, ADAM22 and Caspr2) are linked to Kv_1 channel complex. Overall, the functions of CAMs at the AIS are not well-understood [33]. NF has been shown to recruit the extracellular molecule brevican to the AIS. It is important to mention that the AIS is endowed with a specialized brevican-containing extracellular matrix [19].

Even though the AIS possess well-defined main components, there is remarkable diversity in AIS composition and structure, reflecting the physiologies of different neuronal cell types [30]. It is also important to mention that the AIS is stable but not static. Modulation of AIS structure and function is achieved by posttranslational modifications to AIS components, including

phosphorylation by a number of kinases [30]. Of interest, the AIS and the nodes of Ranvier have common molecular organization [34].

3.2. The importance of the AIS to neuronal polarity

Although the AIS may not be required to axonogenesis, it undoubtedly contributes to the maintenance of neuronal polarity [35]. Indeed, upon AIS dismantlement, the axon loses its identity and acquires many of the molecular and structural features of dendrites [18].

Evidence shows that the AIS contains a physical barrier for lateral diffusion of membrane lipids and proteins that restrict their membrane diffusion to somatodendritic or axonal domains [36, 37]. A model was proposed where a subset of immobilized AIS membrane proteins, likely ion channels and CAMs, functions as 'pickets' that slow the diffusion of membrane proteins and lipids [38].

A physical barrier also exists in the cytoplasm of the AIS. This intracellular filter prevents the cytoplasmic diffusion of large macromolecules and is abolished by disrupting actin filaments and by downregulating AnkG [39]. On the other hand, it was shown that vesicles carrying either dendritic or axonal proteins equally enter to axons and dendrites. However, once in the AIS, almost all dendritic cargoes are halted, and many reverse direction and move toward the cell body. Importantly, the rerouting that occurs in the AIS depends on Myosin Va and intact actin filaments [40]. Indeed, actin patches present along the AIS have been proposed to be responsible for preventing dendritic cargoes from entering into the axon [41]. A second hypothesis suggests that kinesins play a role in selective transport because they preferentially interact with microtubules from either dendrites or axons. However, not the kinesin itself but the kinesin-cargo complex as a whole seems to be responsible for its own selective transport [42].

In summary, many experiments confirm the existence of both a diffusion barrier and an intracellular filter at the AIS. These are undoubtedly crucial to the maintenance of an asymmetric distribution of proteins ad lipids and, consequently, neuronal polarity [35]. Nevertheless, the key mechanisms through which the AIS maintains axonal identity remain unclear.

3.3. AIS plasticity

Although the AIS has originally been considered a static structure, recent evidence suggests that its properties may be plastic [30]. The AIS is the region where somatodendritic inputs are integrated and action potentials are generated [14]. Consistent with this role, recent studies

have showed that AIS structure changes to compensate for alterations in neuronal activity, and so it may work as a homeostatic mechanism [43].

Kuba *et al*. (2010) removed the cochlea of chicks to deprive auditory neurons from synaptic input. In response, AIS length, defined by the distribution of Nav channels and AnkG, increased by 1.7 times, without changes in the types and density of Nav channels expressed. Additionally, membrane excitability and spontaneous firing also increased [44]. In another study, Grubb and Burrone (2010) increased the activity of cultured hippocampal neurons using either high extracellular K^+ concentration to cause chronic depolarization or channelrhodopsin-2 to induce neuronal firing based on photostimulation. In both cases, the AIS relocated, i.e., shifted its location to a more distal position, which resulted in decreased neuronal excitability. Importantly, AIS relocation was a bidirectional phenomenon: the AIS moved proximally after neurons were returned to baseline activity conditions [43]. In summary, these studies suggest that there are two forms of AIS plasticity: resizing and relocation. Unlike resizing, AIS relocation has yet to be reported under any conditions *in vivo* [45].

The effects of electrical activity levels on AIS plasticity depend on the cell type [46]. Nevertheless, the molecular mechanisms regulating the position and length of the AIS only recently started to be unraveled [45]. Determining how the AIS is assembled and maintained will probably be useful to elucidate the mechanisms regulating AIS plasticity [43].

3.4. The importance of the AIS to human diseases

Given the importance of the AIS to action potential generation and maintenance of neuronal polarity, it is not surprising that neurological disorders can arise as a result of AIS dysfunction. Mutations in the gene encoding AnkG have been linked to bipolar disease, schizophrenia, intellectual disability, attention deficit disorder, and autism spectrum disorder [47]. Other AIS proteins have also been implicated in neurological disorders. Caspr2 has been identified as a major susceptibility locus for autism spectrum disorders [47], while several genes encoding AIS ion channels are associated with epilepsy [48]. On the other hand, in a mouse model of the disorder Angelman syndrome, hippocampal neurons had a longer AIS when compared to wild-type mice [49]. Finally, it was recently shown that ischemic neuronal injury causes rapid AIS disassembly and loss of neuronal polarity [14]. Overall, a full understanding of the AIS roles in nervous system diseases may lead to novel disease-specific therapeutic interventions.

II. The Pseudo-Unipolar Morphology and the Proximal Segment

Pseudo-unipolar neurons possess a remarkably unique morphology, since they have a stem process which forms a T-junction by dividing into two axons. Examples of this neuronal type are interneurons and neurons from the cranial nerve sensory ganglia, the trigeminal mesenphalic nucleus and the DRG neurons [50].

DRG neurons have been extensively studied because of their key role in the transmission of sensory signals. Their morphology is of utmost importance for their function and alterations may lead to pathology. As so, new insights on the establishment of this morphology may lead to the development of new therapeutic approaches. Here, we provide an overview of the heterogeneous populations of DRG neurons. We also review current knowledge of the fine structure of DRG neurons, highlighting the ultrastructural differences between the central and peripheral axons. Since these axons present very distinct functional properties, we also present recent knowledge concerning the PS of cultured DRG neurons, which may be a key region in the establishment of neuronal polarity and central-peripheral asymmetry.

1. The Function of DRG Neurons

In vertebrates, all sensory pathways (with the exception of those coming from the head) begin with the activation of the peripheral receptors of DRG neurons [51]. The cell bodies of DRG neurons are located at DRGs, which are paired ganglia located alongside the spinal cord. These neurons possess two axons, a peripheral axon which joins the spinal nerve and projects to a peripheral target, and a central axon that terminates in the CNS. The action potential is generated at the peripheral terminal and conducted along the axons of each DRG neuron towards the CNS.

The central axon enters the spinal cord via the dorsal roots. Then, it can enter one of three anatomical systems. In the dorsal column-medial lemniscus pathway (fig. 5A), the central axon enters an ascending fiber tract in the dorsal white matter and synapse with second order neurons at the dorsal column nuclei of the medulla. This ascending sensory pathway relays predominantly

conscious perception of mechanoreception and proprioception. In contrast, the somatosensory pathways to the cerebellum relay primarily proprioceptive information that does not reach conscious levels. Finally, anterolateral somatosensory pathways (fig. 5B) relay predominantly conscious perception of pain and temperature. In somatosensory pathways to the cerebellum and in the anterolateral system, the central axon of DRG neurons terminate in the spinal grey matter, where it synapses with second-order neurons, interneurons or motor neurons [51]. Afferent fibers mediating pain, temperature and mechanical stimuli terminate in different but partially overlapping laminae of the dorsal horn; whereas proprioceptors synapse in the intermediate zone of the spinal cord and in the ventral horn (fig. 5C) [52].

2. Diversity among DRG Neurons

Sensory neurons represent a remarkably diverse and complex population. They can be classified on the basis of their morphology, conduction velocity, sensory modality, peripheral targets, intensity of stimulus necessary to activate them and neurochemical phenotype.

2.1. Morphology of the Cell Body

Historically, it was generally accepted that there were two main categories of sensory neurons in rat and mouse DRGs based on cell body size: large light neurons of type A and small dark neurons of type B [53]. The "light" cells contain clumps of Nissl substance (clusters of ribosomes and rough ER) interspersed with lightly staining regions of the cytoplasm. In contrast, the "dark" cells have more even and denser distribution of Nissl substance [53]. However, this may be oversimplification as there are many cells with an intermediate size and there is an overlap in the normal size distributions of both neuronal populations [54, 55]. Besides, DRG neurons show great variability in the distribution and three-dimensional configuration of intracytoplasmic organelles, namely the ER, mitochondria and Golgi apparatus. As so, further subtypes were proposed according to ultrastructural features [56].

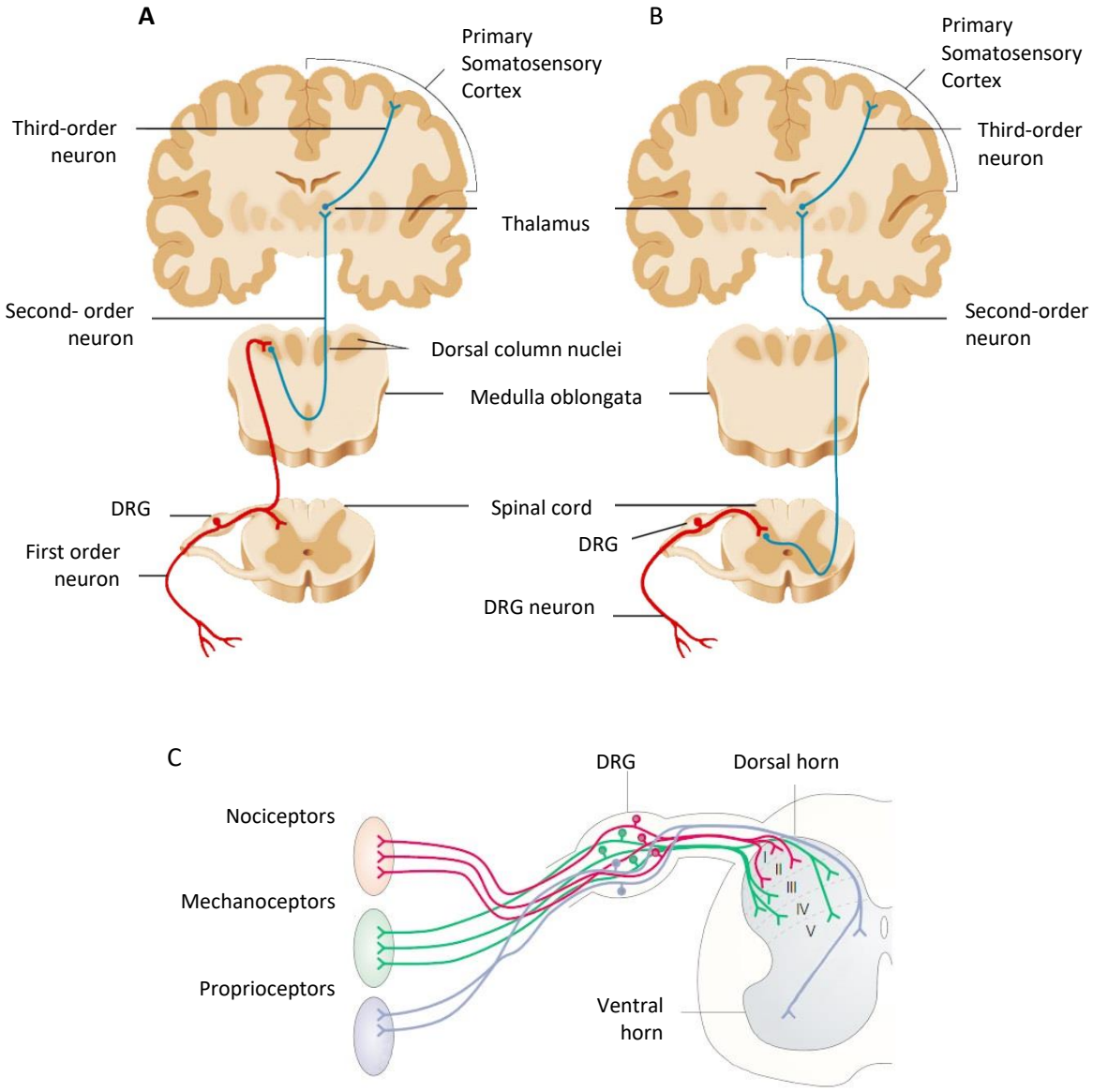

Fig. 5. Ascending somatosensory pathways. (A) Representation of the dorsal column-medial lemniscal pathway showing the DRG neuron synapsing with a second-order neuron at dorsal column nuclei. (B) Representation an anterolateral pathway (the Spinothalamic tract pathway), highlighting the termination of DRG neurons at the grey matter of the spinal cord. Adapted from [57]. (C) Scheme of the organization of the spinal cord in embryonic mouse showing the projections of DRG neurons to specific laminae in the grey matter. Adapted from [58].

2.2. Fiber Conduction Velocity

Signal conduction velocity depends on whether or not the axon is myelinated, and positively correlates with axon diameter [54]. Additionally, some studies have showed that there is a loose positive correlation between cell body size and conduction velocity [59]. As so, it cannot be assumed that large cells give rise to myelinated fibers and small cells to unmyelinated fibers [54].

There are two classical classifications of primary afferents based on conduction velocity of fibers [60]. In mammals, cutaneous, visceral and joint afferent nerve fibers are classified as either Aα, Aβ, Aδ and C, as conceived and revised by Gasser [61]; whereas muscle afferents are classified into group I, II, III and IV fibers, as conceived by Loyd and Chang [62]. The values of signal conduction velocity that distinguish different fiber types vary with species [60]. However, the features of each type of fiber are consensual. Aα/group I and Aβ/group II fibers are large-diameter and myelinated and have high conduction velocities. In contrast, Aδ-type/group III fibers are medium sized and lightly myelinated and have intermediate conduction velocities. Finally, C-type/group IV fibers are unmyelinated and have the smallest diameter and the slowest conduction velocity [63].

Importantly, conduction velocity of sensory neurons is not a reliable indicator of their functional category. In fact, no category of fiber conduction velocity defines a unique type of sensory unit [60].

2.3. Sensory Modality

DRG neurons can be further classified into four heterogeneous groups based on sensory modality: nociceptors, mechanoreceptors, proprioceptors and thermoreceptors.

Nociceptors are responsible for pain and respond preferentially to damaging (noxious) or potentially damaging stimuli, which include chemical, thermal (hot and cold) and mechanical modalities. They are divided according to the modality of stimulus or combination of stimuli they respond to [64]. They may have C-, Aδ-, or Aβ-fibers, although the latter is often ignored in the literature [65].

Mechanoreceptors are sensory neurons that respond to mechanical pressure or distortion. While high-threshold mechanoreceptors are nociceptors, low-threshold mechanoreceptors mediate innocuous stimuli [66]. Cutaneous mechanoreceptors are divided into four types based on the physiological properties in response to sustained mechanical stimulation [67]. Mechanoreceptors projecting to the skin may have Aα-, Aβ-, or C-type fibers [66].

The term proprioception may be interpreted as the perception of body position and movements in three-dimensional space [68]. Proprioception is mediated by specialized mechanoreceptors, mainly muscle spindle primary endings (Ia afferent fibers). Additionally, muscle spindle secondary endings (II afferent fibers), Golgi tendon organs (Ib afferent fibers) and joint and skin mechanoreceptors also contribute to proprioception [69].

Thermoreceptors are primary afferent fibers that mediate non-painful thermosensation, namely innocuous cold or warmth. They are classified as cold or warm fibers, since they seem adapted to convey information over a particular temperature range. Thermoreceptors may have Aδ-, or C-type fibers. Interestingly, a DRG neuron can be simultaneously a mechanoreceptor and a thermoreceptor [70].

2.4. Neurochemical Phenotype

The molecular properties of sensory neurons have been extensively studied, particularly their expression of various receptors, ion channels and transcription factors. However, the defining molecular characteristics of sensory neuron types are not completely understood [52] and so traditional neuron subset-specific markers label multiple neuron types [71]. For instance, C fiber neuron subtypes are traditionally defined into two classes based on molecular properties. The peptidergic group expresses neuropeptides such as substance P or calcitonin gene related-peptide; whereas the non-peptidergic class is marked by isolectin IB_4. However, these traditional classes show overlap and do not account for the entirety of C fiber neurons. Moreover, some of these markers are found in other types of neurons [72].

2.5. New Classifications of DRG Neurons

There is still not a consensual classification for DRG neurons based on most of the criteria mentioned in the previous sections, because DRG neuron classes can only be defined by integrating functional, transcriptomic and morphological features [71]. New classifications of DRG neuronal types are emerging due to advances in single-cell transcriptomics that have allowed the integration of functional cell-type identity with the gene expression profile of individual neurons [71, 73].

3. Pseudo-Unipolarization of DRG neurons

Sensory ganglion neurons are pseudo-unipolar [74], with the exception of vestibular and spiral ganglion neurons [75]. They possess a stem process which forms a T-junction by dividing into two axons: a central axon that terminates in the CNS and a peripheral process which projects to a peripheral target.

During their early embryonic development, DRG neurons are bipolar and undergo a unique morphological change, termed pseudo-unipolarization, to assume their mature form. Pseudo-unipolarization was first mentioned by His (1886) and first described in detail by Ramón y Cajal (1904) [76, 77]. This phenomenon was examined *in vivo* using classical silver impregnation methods [74, 76] and later confirmed using scanning electron microscopy [78, 79], transmission electron microscopy [80], retrograde tracing techniques [81], and immunohistochemistry for cytoskeletal markers [82].

Ramón y Cajal (1955) summarized the histogenesis of developing neuroblasts of the DRGs as follows (fig. 6) [83]. In early stages, most DRG neurons are spindle-shaped bipolar. As the cell body bulges more in a direction, the two processes approach each other forming an angle less than 90 degrees (bell-shaped bipolar conformation). Then, the cell body elongates and constricts between the initial segments of the two processes to form the stem process from which the two axonal processes protrude [75]. In some textbooks of histology, pseudo-unipolarization of DRG neurons is described as deriving from the fusion of two opposing processes. However, the mechanism of pseudo-unipolarization has not been conclusively reported [84]. In fact, many authors proposed the hypothesis of the cell body elongation for pseudo-unipolarization, but neither hypothesis have been confirmed [75, 84].

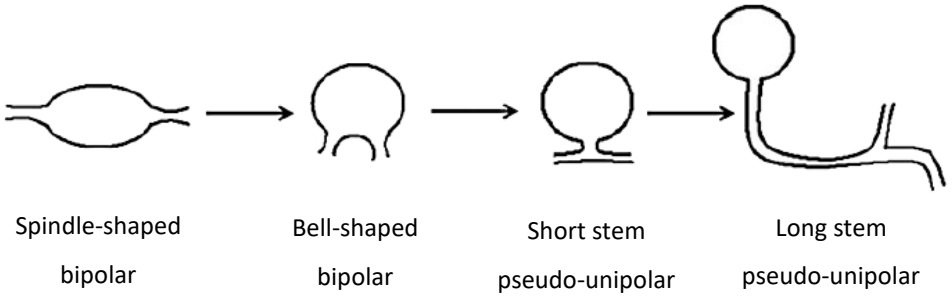

Fig. 6. Morphological changes leading to a pseudo-unipolar structure. Adapted from [85].

The time of onset of pseudo-unipolarization depends on the species. In rats, at embryonic day (E) 14, only 7% of neurons are pseudo-unipolar, while at E19 this percentage has abruptly increased to 94% [78]. In mice, on E12, all DRG neurons are bipolar whereas the bell-shaped bipolar and pseudo-unipolar neurons are predominant at E15 [81]. On the other hand, in chicks, pseudo-unipolar neurons were detected after E6 and increased in number to 53% on E14 and 82% at 2 days after hatching [78].

In vitro, it was shown that pseudo-unipolarization requires the presence of glial cells [86], and more specifically the contact between DRG neurons and Schwann cells [87].

4. Fine Structure of DRG Neurons

4.1. Neuron Cell Body

In DRGs, clusters of neuron cell bodies are interspersed among nerve fascicles. In cross sections, the neuronal clusters appear to assume different sizes and shapes. Each cluster of neuron possesses cells of different size and there appears to be no specific pattern in their arrangement [88]. DRG neurons are typically circular to oval in outline and are of variable size ranging from 20 to 100μm in diameter in rats [54].

The cell bodies of DRG neurons are completely wrapped by sheaths comprised of several satellite glial cells (SGCs). These perineural sheaths may have one or several layers of SGCs, are generally continuous and have the outer surface covered by a basal lamina [89]. Importantly, each neuron and its surrounding SGC sheath constitute a morphological unit which is separated from other units by connective tissue. There are gap junctions coupling SGCs within each perineural sheath and also SGCs belonging to different perineural sheaths, but the latter case occurs only after injury. However, so far no gap junctions were described between the neuron cell body and its attendant satellite cells. Occasionally, there are two or three neuron cell bodies, in most cases separated from each other by a SGC sheath, sharing a common connective envelope [89].

The surface of vertebrate DRG neurons has many slender perikaryal projections which were first thought to be a technical artifact [90]. These projections are present over the soma and stem process surface (fig. 7A) [91]. Their outgrowth is influenced by the perineuronal microenvironment, since they are abundant in neuronal surface domains covered by satellite cells or other neurons [92] but are absent from regions in direct contact with the extracellular matrix

[93]. Perikaryal projections are believed to be important for neuronal metabolism by increasing the surface area available for exchange of metabolites [94].

One interesting feature of DRG neurons is the terminal Dogiel's nest, which was first described in the late nineteenth century (fig. 7B) [95]. Terminal Dogiel's nests are endings of unmyelinated sympathetic fibers typically with a diameter inferior to 1µm that either present the shape of a nest or a plexus enveloping the SGCs sheath [96]. These sympathetic fibers can penetrate the area between the SGCs sheath and neuron cell body and may establish synaptic contacts with DRG neurons [97, 98]. The number of terminal Dogiel's nests increases with increasing phylogenetic complexity and, in rats, their number increases with increasing age and is greater around larger complexes of neurons and SGCs sheath [96, 99]. Strikingly, following nerve injury, perivascular sympathetic endings emit sprouts and penetrate those DRGs containing the cell body of axotomized neurons, to end up forming terminal Dogiel's nests [100]. Accordingly, electrophysiological studies show that peripheral nerve injury triggers functional sympathetic–sensory coupling in DRGs [101]. Furthermore, neurons which modulate sympathetic outflow to DRGs receive primary sensory afferents from corresponding DRGs [102]. As so, sympathetic sprouting in the DRG has been suggested as an important underlying mechanism for neuropathic pain [102].

4.2. Stem Process

The stem process is the portion of the axon between the cell body and the bifurcation into central and peripheral processes, and may be hundreds of micrometers in length [103]. While the proximal region of the stem process is always unmyelinated and ensheathed by SGCs, the distal part is ensheathed by Schwann cells and is myelinated if axonal processes are myelinated [104-107]. In higher vertebrates, the proximal portion of the stem process may form the initial glomerulus of Cajal, which consists of a stem process making a tortuous, coiled path, and eventually spiraling around the SGCs sheath, with a diameter typically superior to 1µm (fig. 7C) [96, 105]. The initial glomerulus of Cajal is more common in larger neurons [105] and is ensheathed by SGCs [108].

The unique ultrastructure of the stem process of DRG neurons was studied in the twentieth century in many species, including rabbits [80, 106], cats [104, 106], frogs [108], rats [103, 106, 107], monkeys [106] and also in culture [109]. An overview of the fine structure of the stem process is provided in detail below.

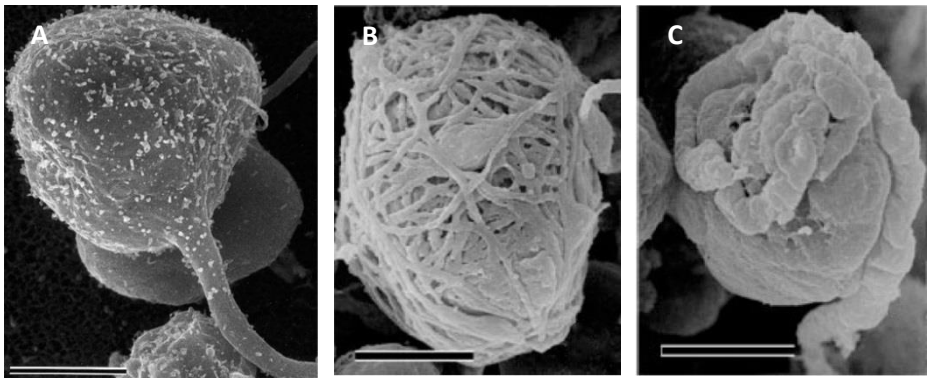

Fig. 7. Scanning electron micrographs showing the three-dimensional cytoarchitecture of DRG neurons. (A) Perikaryal projections of post-natal rabbit DRG neurons, seen after removal of the satellite glial cell (SGC) sheath. Scale bar, 10µm. Image from [91]. (B, C) Scanning electron micrographs of the exposed surface of the rat DRG, showing an intricate meshwork of sympathetic fibers forming a Dogiel's nest (B) and a highly convoluted stem process forming an initial glomerulus of Cajal (C), covering their respective parent neurons and satellite glial cell sheaths. Scale bars, 50µm. Images from [96].

The cytoplasm of the stem process (fig. 8) contains strikingly larger numbers of mitochondria, dense bodies [106, 107], and ribosomes [106, 107, 110], and higher density of microtubules and ER [107] than seen peripherally. The numbers or densities of these organelles diminishes with increasing distance from the cell body [107]. Regarding the surface membrane, the proximal non-myelinated stem process has many perikaryal projections; whereas the surface membrane ensheathed by Schwann cells is smooth, as seen peripherally [107].

In the proximal part of the stem process, microtubules are closely packed in fascicles and connected with lateral cross bridges (fig. 8B) [107, 109, 111]. Additionally, Zenker and Högl (1976) also observed a thin layer of dense material undercoating the axolemma, beginning in the most distal unmyelinated region and ending abruptly at the first heminode (fig. 8A) [107]. These ultrastructural features are similar to those of the AIS of multipolar neurons, which is characterized by fasciculated microtubules and a thin lamina of electron dense material beneath the axolemma [112].

The first internodes of the stem process are, in proportion to the axon diameter, unusually short and thinly myelinated [106]. Besides, the myelin sheath is surrounded by an outer coat of flattened SGCs processes which is separated from the myelin sheath by a layer of connective tissue [107].

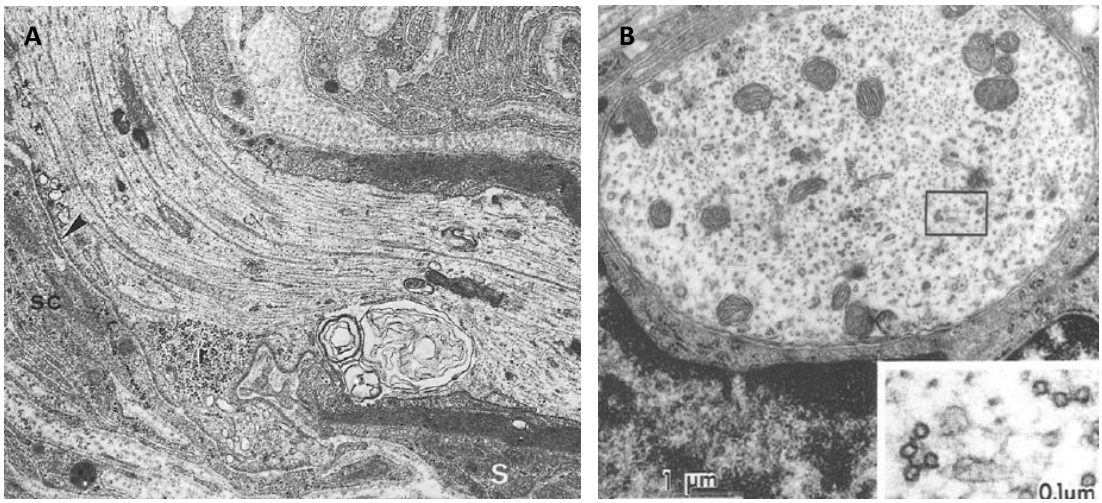

Fig. 8. The ultrastructure of the stem process. (A) Longitudinal section through the terminal part of the unmyelinated portion of the stem process and through the first heminode. The arrow indicates the axolemma, which in this region is undercoated by dense granular material, according to Zenker and Högl (1976). Neurofilaments, microtubules and mitochondria are axially oriented. *S*, Schwann cell cytoplasm, *sc*, satellite cell leaflets, *r*, ribosome-like particles. X 18 800. Image from [107]. (B) Transversal section of the unmyelinated portion of the stem process proximal to the myelinated portion. Fasciculated microtubules are frequent, as shown at a higher magnification in the inset. There is no layer of dense material undercoating the axolemma. Image from [111].

At the bifurcation, neurofilaments and microtubules divide into two streams, one to the peripheral process and the other to the central one. No neurofilaments or microtubules traverse between both processes [104]. In addition, the bifurcation has fasciculated microtubules [111], multivesicular bodies and a triangular area which is occupied by clusters of mitochondria [104]. The bifurcation of myelinated fibers is constricted and has a node of Ranvier, while unmyelinated fibers show a triangular expansion at this region [104].

4.3. Axonal Processes

Both the peripheral and central axonal processes branch extensively at the terminal fields but rarely in or near the ganglion [113]. In unmyelinated fibers of the same DRG neurons, central processes have smaller diameter than the peripheral ones [54, 114]. However, in the case of myelinated fibers, there is not consensus as to whether there is a size difference between central and peripheral processes [54, 114]. In fact, it has been reported that myelinated central and

peripheral processes are approximately equal in size [104, 115] but it has also been claimed that myelinated central processes are smaller than peripheral ones [54, 114].

Myelinated axons are surrounded by a Schwann cell sheath, which includes the myelin sheath and is encircled by basal lamina [116]. Unmyelinated fibers are scattered among the myelinated ones (fig. 9). Most unmyelinated axons are enveloped singly by their Schwann cell, and occasionally more than one axon shares the same Schwann cell sheath. The complex of Schwann cell sheath and its associated unmyelinated axon(s) is known as Remak bundle and is encircled by basal lamina. Moreover, some regions of the plasma membrane of unmyelinated axons are covered directly by basal lamina [117]. Interestingly, the cross-sectional area of the Schwann cell sheath is directly proportional to that of its related axon, in the case of both myelinated and unmyelinated fibers [116, 117].

At the region immediately distal to the bifurcation, the central and peripheral processes share the same ultrastructural features, both possessing the characteristics of an axon [104]. However, some structural differences have been reported between the two processes more distally, although not in a consensual way.

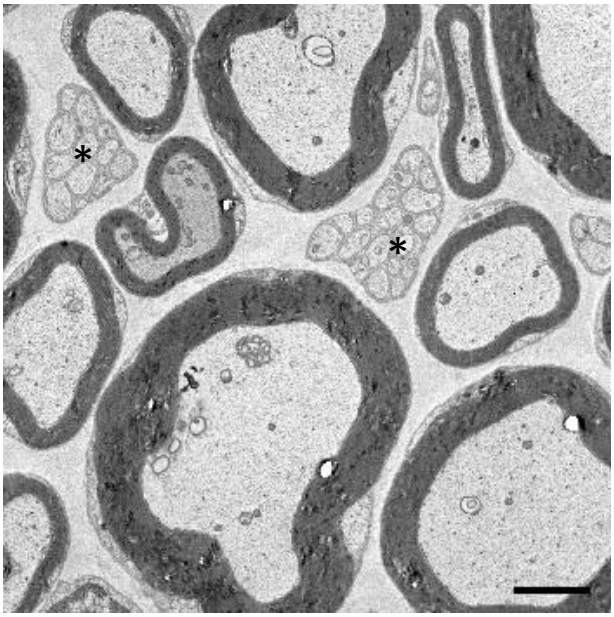

Fig. 9. Axonal organization in the peripheral nerve . Electron micrographs of sciatic nerves of 1.5-year-old mice showing unmyelinated, small myelinated, and large myelinated axons. Asteriks indicate Remak bundles containing several unmyelinated axons. Scale bar, 2µm.

Both axonal branches possess axially oriented mitochondria, microtubules and neurofilaments, such as the stem process. The density of microtubules decreases with an increase of axon diameter [118, 119] and is higher in close proximity to mitochondria [119]. According to some studies, the density of microtubules is significantly higher in myelinated peripheral processes than in myelinated central processes of a similar size [118, 120]. However, in a different study, the slopes of microtubule density as a function of fiber diameter on either side of the ganglia were closely similar [115]. In contrast, in unmyelinated nerve fibers, the density of microtubules is significantly higher in peripheral processes than in central processes of similar size [118]. Interestingly, some microtubules are arranged in fascicles at nodes of Ranvier, and the density of fasciculated microtubules is higher in axon portions more proximal to the cell body [111].

Regarding neurofilaments, myelinated fibers have approximately the same density of these structures in both processes [115, 120], whereas unmyelinated fibers have a smaller density of neurofilaments in the peripheral process than in the central one [115]. Moreover, this density did not change as a function of nerve fiber diameter [115, 120].

In the peripheral process of myelinated fibers, the smooth ER forms a continuous tridimensional network which is suggested to extend from the perikaryon to the axon terminals [121]. Nevertheless, free vesicles and tubular fragments also exist and are more frequent at the node of Ranvier [121]. Additionally, the ER shows polarity, with most tubules running parallel to the axon [121, 122]. In myelinated fibers, peripheral processes possess slightly more ER than the myelinated central processes [120]. Accordingly, during the bell-shaped bipolar stage of rabbit neuroblasts, the proximal region of the two processes differ: one process contains a small amount of ER and therefore resembles an axon, while the other contains a considerable amount of granular ER typical of dendrites [80]. However, in this study the authors were not able to determine which processes originate the central and peripheral axons.

Ribosomes were shown to be absent from the central process either near the ganglion or at its entrance in the spinal cord, but were present in intraganglionar axons and in the peripheral process near the ganglion [110]. In a later study in rabbits, it was shown that a large number of ribosomes are confined to a few peripheral processes only, near the ganglion [123]. Additionally, these organelles were more often seen near the axonal membrane than in the axial regions and frequently in the vicinity of mitochondria [110, 123]. Ribosomes were usually arranged in clusters and only occasionally in close attachment to the ER [110, 123].

It is important to note that the axonal diameter and the distribution of organelles are not homogeneous along the length of myelinated axons (fig. 10). In fact, internodes have a larger cross-sectional area than the nodes of Ranvier [103, 122]. On the other hand, dense lamellar bodies, axoplasmic granules [122] and vesicular-tubular organelles [103, 122] are mostly located in paranode-node-paranode regions and rarely in internodes. Moreover, the node of Ranvier has less neurofilaments and denser microtubules comparing to its internode [103].

Although the axolemma of unmyelinated fibers is homogeneous, in myelinated fibers the axolemma possess regional specializations at and around the node of Ranvier [124]. In DRG neurons, the nodal axolemma possess an electron-dense layer on its axoplasmic side (fig. 10A) [103, 125], and its surface area is increased by outgrowths and invaginations [125].

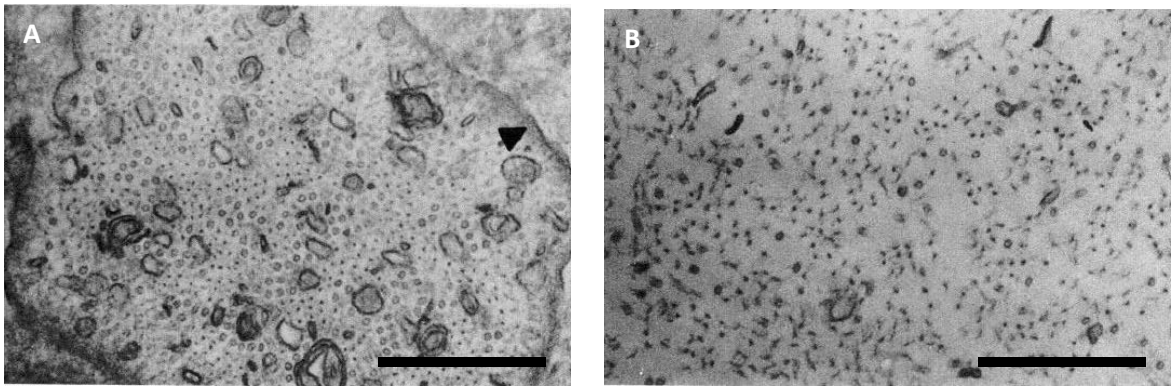

Fig. 10. Ultrastructural differences between the node of Ranvier (A) and its internode (B) . Note the electron-dense undercoating of the nodal axolemma (arrowhead in A). The node of Ranvier (A) has a lower number of neurofilaments and a higher density of microtubules and vesicular organelles comparing to its myelinated internode (B). Scale bars, 0.5 µm. Images from [103].

5. Functional Asymmetry of Central and Peripheral Axons

Besides structural features, the central and peripheral processes of DRG neurons present different functional characteristics. However, it is not known what ultrastructural differences justify the strikingly different functional properties between the central and peripheral axons. The most remarkable asymmetric feature is due to the direction of signal conduction. The peripheral process is dendrite-like, since the action potential is generated at the its peripheral terminal and propagated towards the bifurcation of the stem process; whereas the central process is axon-like, since it conducts the signal from the bifurcation to the CNS [126].

DRG neurons have more central-peripheral asymmetry regarding electrophysiological properties. Signal conduction velocity is higher in the myelinated peripheral process than in the myelinated central process of the same cell [54, 127]. An additional and interesting asymmetry is that conduction velocity of both branches decreases after axotomy of the peripheral process, whereas section of the central process increases the conduction velocity of only the peripheral process [128].

The two axonal processes also show asymmetry regarding protein transport. The flow rate of fast transport is identical between the central and peripheral processes [129], but the amount of rapidly migrating proteins within the central process is clearly less as compared with the peripheral axon [115]. Regarding the slow axonal transport, both its rate and the amount of slowly migrating protein are higher in the peripheral axon comparing to the central process [130, 131].

Notably, the rate [131] and extent [132] of regeneration of the peripheral process is higher than that of the central one. The environment created by Schwann cells in the peripheral nerve contributes to its successful regeneration [132]. However, the differential regenerative capacity is not only due to extrinsic differences [133]. In any case, peripheral and central axotomies have different effects on DRG neurons [134]. An injury to the peripheral axon enhances the regeneration of both the peripheral and central axons, while a central injury fails to induce regeneration on either [132].

6. The Proximal Segment

In cultured DRG neurons, the PS of neurites has a different composition when compared to the rest of the neurites. *In vitro*, the PS is enriched in AnkG [135], βIV-Spectrin [13, 19], Nav channels [34] and NF [34, 135]. Therefore, the PS has a molecular composition similar to the AIS and nodes of Ranvier [34]. The PS, as defined by enrichment in at least one of these components, in DRG neuron cultures is located in the initial portion of some neurites of multipolar cells [34] and also in the stem process of apparently pseudo-unipolar DRG neurons [13, 19].

The AIS is a specialized ~20–40-µm-long structure located in the proximal axon of multipolar neurons [13] that undoubtedly contributes to the maintenance of neuronal polarity [35]. Indeed, upon AIS dismantlement, the axon loses its identity and acquires many of the molecular and structural features of dendrites [18]. Since the PS has a molecular composition and

localization similar to the AIS, it may contribute to the pseudo-unipolar morphology or to the central-peripheral polarity of DRG neurons.

The defining molecular component of the AIS is AnkG. This is the first AIS component to cluster and is required for the recruitment of many other AIS components [19]. In DRG neurons, the existence of the PS *in vivo*, as defined by enrichment in AnkG, was not yet shown. In contrast, it was shown *in vivo* that AnkG is enriched at the nodal membrane of DRG neurons [136]. During early development, AnkG is distributed along the length of axons. Later, AnkG disappears from unmyelinated processes; whereas in myelinating axons, AnkG redistributes to a highly polarized localization at clusters which later form the nodes of Ranvier [136].

Importantly, the PS and nodes of Ranvier of DRG neurons are two types of axonal domains that assemble by very different mechanisms [34]. During development, neuron-glia interactions lead to the formation of clusters containing NF along the length of the axon [137]. NF recruits AnkG which, in turn, is responsible for the subsequent localization and assembly of nodes of Ranvier [34]. Interestingly, in the absence of AnkG, other proteins rescue nodal assembly [138]. In contrast, NF is not necessary for clustering of AnkG at the PS of cultured DRG neurons [34]. In fact, AnkG can be targeted to the PS by multiple regions, suggesting that distinct protein interactions may be involved [135]. However, it is still unknown how AnkG concentrates at the PS [34]. According to Zhang and Bennet (1998), the assembly of PS does not require the presence of glial cells and so is intrinsically specified [135]. Similarly, the AIS is intrinsically assembled by multipolar neurons [15]. In contrast, node formation requires neuron-glia interactions and so is not intrinsically specified by the axon [137].

CHAPTER 2

Axon Initial Segment Plasticity

I. Objectives

The main focus of this work was to understand the mechanism of AIS relocation in response to chronic depolarization, in dissociated hippocampal neuron cultures. We specifically aimed at understanding if the AIS is assembled *de novo* or if its pre-existing components move along the axon. As so, the following approaches were performed:

- We used protein synthesis inhibition to understand the importance of *de novo* protein synthesis in AIS relocation;
- We used gene silencing of stable AIS components to understand if the AIS needs newly synthetized molecules to relocate.

II. Materials and Methods

Hippocampal Neurons Culture

Hippocampal neurons were isolated from E18 Wistar rats. For that, pregnant females were euthanized by carbon dioxide inhalation. Absence of heart beat was assessed and decapitation was used as a confirmatory method. Then, the euthanized rat was laid in dorsal recumbency on a clean pad, and the abdomen was sprayed with 70% ethanol. The abdominal wall was cut medially with scissors to expose the uterus, which was placed in a sterile Petri dish containing physiological saline solution. Using forceps, the amniotic sac of each embryo was removed. Then, embryos were maintained in ice cold Hanks' Balanced Salt solution (HBSS, Sigma-Aldrich) until dissection.

The embryos were decapitated using scissors and the dissection of hippocampi was performed under a dissection microscope with a pair of fine forceps (fig. 11). Briefly, the brain (fig. 11A) is carefully dissected out from the skull and placed in a Petri dish containing HBSS. Then, a sagittal incision is made to harvest the two hemispheres (fig. 11B,C). Each hemisphere is placed medial side up (fig. 11D). Then, diencephalon is removed to expose the medial side of the hippocampus. Finally, the meningeal tissue is removed (fig. 11E) and the hippocampus is dissected out (fig. 11F). Hippocampi are stored in ice-cold Neurobasal medium (Invitrogen) until further processing.

Hippocampi were digested with 0.05% porcine trypsin (Sigma-Aldrich) in HBSS for 15 min at 37°C. Then, trypsin was substituted by a 10% fetal bovine serum (FBS, Invitrogen) in HBSS for 5 min at room temperature. Hippocampi were then washed twice with HBSS and once with Neurobasal medium. Finally the tissues were resuspended in 1 ml of final medium (Neurobasal medium containing 2% B27 (Invitrogen), 2 mM l-glutamine (Invitrogen), and 1% penicillin–streptomycin (P/S, Invitrogen)) and then dissociated by pipetting up&down with P1000. The cell suspension was filtered with a 70µm strainer and finally neurons were seeded in 24-well plates with glass coverslides coated with poly-L-lysine (20µg/mL, Sigma-Aldrich). Cells were maintained in final medium. At the end of each experiment, cells were fixed in 2% paraformaldehyde (PFA, Sigma-Aldrich) for 10 min at room temperature. Cells were then washed and stored in PBS at 4°C.

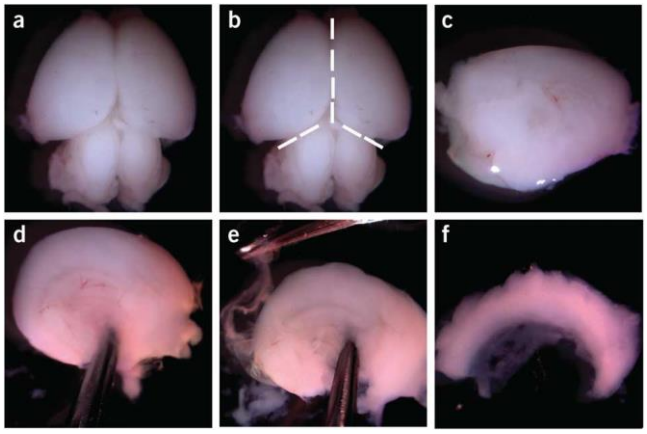

Fig. 11. Steps for dissection of the hippocampus from the intact brain of mouse and rat. Image from [139].

Immunocytochemistry

Previously fixed cells were incubated with 0.1% Triton-X100 (Sigma-Aldrich) in phosphate-buffered saline (PBS) for 5 min, followed by incubation with 200mM Ammonium Chloride (Merck) for 10 min. Cells were washed 3 times with PBS pH 7.4 after each step. Non-specific antibody-binding sites were blocked with 5% FBS in PBS for 1 hour at room temperature and then incubated with primary antibodies diluted in blocking solution overnight at 4°C (table 1). After three washes with PBS, cells were further incubated with the appropriate secondary antibodies for 1 hour at room temperature. Cells were washed with PBS, and the slides were mounted with Fluoroshield containing DAPI (Sigma-Aldrich) and visualized under a fluorescence microscope (Leica DMI6000 B) with a 40x, 0.60 NA objective coupled to a camera (Hamamatsu C11440-22C).

Table 1 – Primary and Secondary Antibodies used in Immunocytochemistry

	Antigen	Type	Host	Dilution	Company [Catalogue Nr.]
Primary Antibodies	AnkG	Monoclonal	Mouse	1:100	Santa Cruz Biotechnology [sc-12719]
	Pan-Neurofascin	Monoclonal	Mouse	1:100	Neuromabs [75-172]
	βIV-Spectrin	Polyclonal	Rabbit	1:250	Kind gift from Prof. M. N. Rasband
	βIII-Tubulin	Monoclonal	Mouse	1:2000	Promega (G7121)
	βIII-Tubulin	Polyclonal	Rabbit	1:500	Synaptic Systems [302302]
Secondary Antibodies	Mouse IgG	AlexaFluor®647	Donkey	1:200	Life Technologies [A31571]
	Mouse IgG	AlexaFluor®594	Donkey	1:500	Jackson ImmunoResearch Laboratories [715-585-150]
	Rabbit IgG	AlexaFluor®488	Polyclonal	1:500	Life Technologies [A21206]
	Rabbit IgG	AlexaFluor®568	Donkey	1:500	Life Technologies [A10042]
	Rabbit IgG	AlexaFluor®647	Donkey	1:200	Life technologies [A31573]

Protein Synthesis Inhibition Assay

Hippocampal neuron cultures were performed as described above, with 25,000 cells plated per well plate. After 10 days *in vitro* (DIV), the medium was collected and cells were incubated with fresh medium with either ethanol (EtOH) or cycloheximide (1µg/ml in EtOH, CHX, Sigma-Aldrich) for 1 hour at 37°C. Then, the collected medium was added back to the wells and 1M of sodium chloride (NaCl, Sigma-Aldrich) or potassium chloride (KCl, Merck) solution was added to each well to obtain a final concentration of 10mM. Cells were then incubated at 37°C for two days and then fixed.

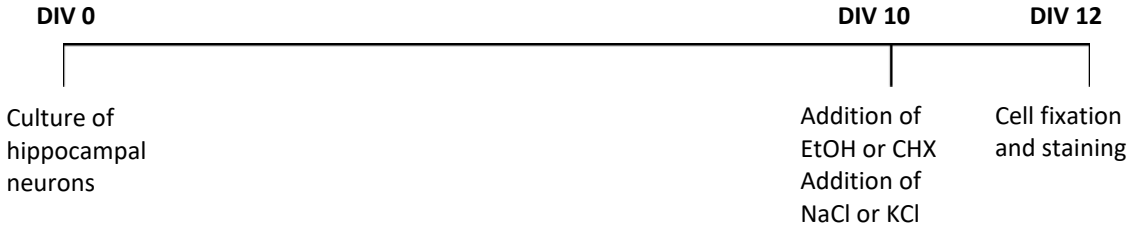

Fig. 12. Scheme of the experiment of protein synthesis inhibition.

Cells were immunostained for AnkG and βIII-tubulin as described above. Image analysis was performed with ImageJ software (Universal Imaging Corp.). AIS location was determined by the region of the axon with AnkG fluorescence intensity higher than 33% of its maximum.

Three independent assays were performed with independent cell cultures, and 45–60 AISs from 2 coverslips were analyzed per experiment for each condition.

Cell Viability Assay

Cell culture was performed and treated with CHX as described above. Two days after treatment, cells were incubated with 1µg/ml calcein (Invitrogen) for 30 min at 37°C, followed by incubation with 10µg/ml propidium iodide (Sigma-Aldrich) for 5 min. Then the medium was replaced by Neurobasal without phenol red (Invitrogen) containing 2% B27, 2 mM l-glutamine, and 1% P/S. Cells were visualized and photographed under a fluorescence microscope (Leica DMI6000 B) with a 10x, 0.25 NA objective coupled to a camera (Hamamatsu C11440-22C). Image analysis was performed using ImageJ to determine the live (calcein positive) and dead cells (propidium iodide positive).

Gene silencing and cell depolarization

βIV-Spectrin and 186-kDa Neurofascin short hairpin RNA (shRNA) plasmids were kindly provided by Matthew N. Rasband (Baylor College of Medicine, Houston). Efficacy and specificity of shRNA sequences were previously demonstrated [19]. The control plasmid contains a sequence directed against a nonmammalian protein; whereas the shRNA expression plasmids contain shRNA for gene silencing of βIV-Spectrin or NF. Each control or shRNA plasmid was co-transfected with pmaxGFP (Lonza), which is a plasmid that promotes the expression of green fluorescent protein (GFP), which serves as a marker of transfected cells.

For these studies, cell culture was performed as described above with 30,000 hippocampal cells plated per well. After 7 DIV, cells were transfected with DNA-calcium phosphate co-precipitates. Briefly, for each well, a 25µl solution containing DNA (1.5µg of shRNA expression plasmids or control plasmids, and 0.5µg of pmaxGFP) and 250mM $CaCl_2$ (Sigma-Aldrich) in Tris-EDTA buffer (TE, 10mM Tris, 1mM EDTA, pH 7.3) was prepared. This mixture was added dropwise to 25µl of 2x HEPES-buffered saline (HEBS, 16g/L NaCl, 0.74g/L KCl, 2g/L glucose, 10g/L HEPES, 0.198 Na_2HPO_4, pH 7.2) . Solutions were vortexed and the precipitate was allowed to develop at room temperature for 30 min, protected from light. Then cell media were collected and 250µl of Neurobasal was added to each well, followed by 50µl of precipitate dropwise. Cells were incubated with the precipitate for 45 min at 37°C. After incubation, the medium containing the precipitate was removed and cells were incubated with acidic Neurobasal (medium previously placed in a 10% CO_2 atmosphere) for 15 min at 37°C in 5% CO_2. Finally, acidic Neurobasal was replaced by the culture media previously collected.

Two days after transfection (DIV 9) cells were treated with NaCl or KCl as described above, incubated for another two days (DIV 11) and then fixed in 2% PFA for 10 min at room temperature.

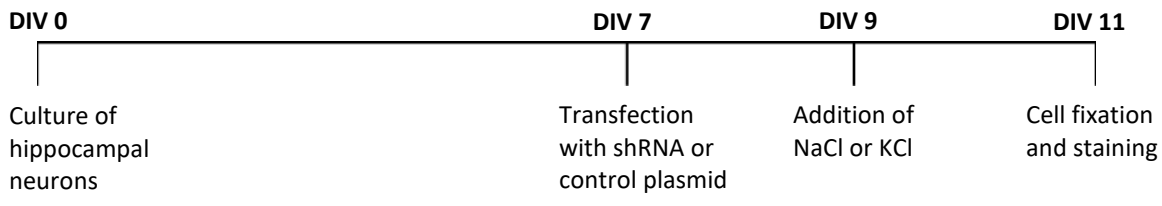

Fig. 13. Scheme of the gene silencing experiment.

Cells were immunostained for βIII-tubulin and AnkG, βIV-Spectrin or NF as described above. Neurons were identified by βIII-tubulin immunolabeling and then the percentage of cells with AIS^+ staining was determined in transfected and non-transfected neurons.

For each immunostaining, at least two independent assays were performed with independent cell cultures. Per independent assay and for each condition, 60 transfected neurons (βIII-tubulin and GFP positive cells) and 80 non-transfected neurons (βIII-tubulin positive and GFP negative cells) were counted.

Statistical analysis

All values are presented as mean±SEM. Statistical analysis was performed using GraphPad Software. For protein inhibition studies, significance was determined using 2-tailed Student's t-test; whereas for shRNA experiments Two-way ANOVA was employed.

III. Results

AIS maintenance and relocation require protein synthesis

To study the effect of *de novo* protein synthesis on AIS plasticity, we treated cells with a protein synthesis inhibitor (CHX) or EtOH (as control). Then we added a high concentration of extracellular KCl for 48h to induce a chronical depolarization of hippocampal neurons, thus promoting AIS relocation [43]. For baseline conditions, a similar concentration of NaCl was added. This approach enabled us to understand whether the relocation of the AIS depends on new protein synthesis or in the movement/recycling of pre-existing components.

In control cells, chronical depolarization led to the repositioning of the AIS (its start position moved ~2.5µm distally when compared to baseline conditions), while CHX treatment impaired AIS relocation (fig. 14B), suggesting that protein synthesis is needed for AIS plasticity. Furthermore, CHX treatment resulted in a shorter AIS when compared to EtOH-treated neurons, both at rest and at chronic depolarization conditions (fig. 14C). These results suggest that CHX treatment is promoting AIS disassembly. To better understand this process, we aimed at determining if a particular region of the AIS was being affected. Interestingly, at rest, the AIS of CHX-treated cells started distally and ended proximally comparing to the control (fig. 14B). At chronic depolarization, the AIS of CHX-treated cells also ended proximally comparing to the control (fig. 14B). Also, we observed an increase in the percentage of fragmented AISs in CHX-treated cells (fig. 14D). Since the affected region of the AIS was very variable, there was not a specific pattern of fragmentation. Consistent with this observation, CHX also induced a decrease in AnkG fluorescence intensity (fig. 14E). This decrease was observed in both rest (NaCl) and chronic depolarization (KCl) conditions. Overall, these results suggest that protein synthesis is needed not only for AIS relocation, but also for AIS maintenance.

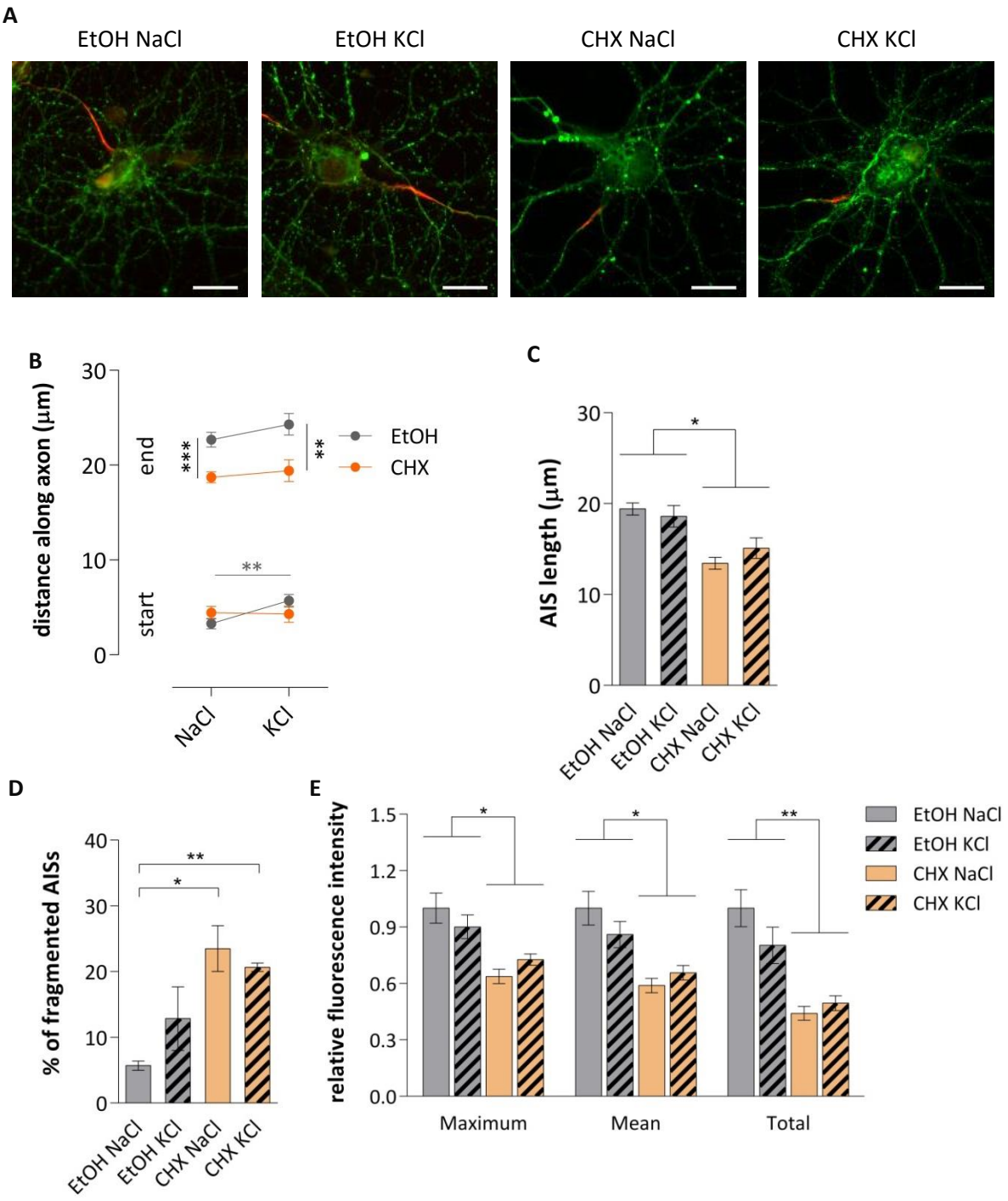

Fig. 14. AIS properties of ethanol- and cycloheximide-treated cells. (A) Representative images of hippocampal neurons treated with EtOH or 1µg/ml CHX, and NaCl or KCl. Cells were immunostained for AnkG (red) to label the AIS and βIII-tubulin (green) to mark neurons. Scale bars, 20µm. (B) Axonal position of the AIS start and end in EtOH- (grey) and CHX-treated (orange) cells. (C) Length of the AIS and (D)

percentage of fragmented AISs. (E) Graph of maximum, mean and total fluorescence intensity levels relative to the fluorescence intensity levels of EtOH- and NaCl- treated cells. *p<0.05, **p<0.01, and ***p<0.001.

To exclude a possible cytotoxic effect from CHX, a cell viability assay was performed. No toxic effect was found in any condition. Cells were viable, i.e., stained with fluorescent calcein dye but not with propidium iodide (fig. 15).

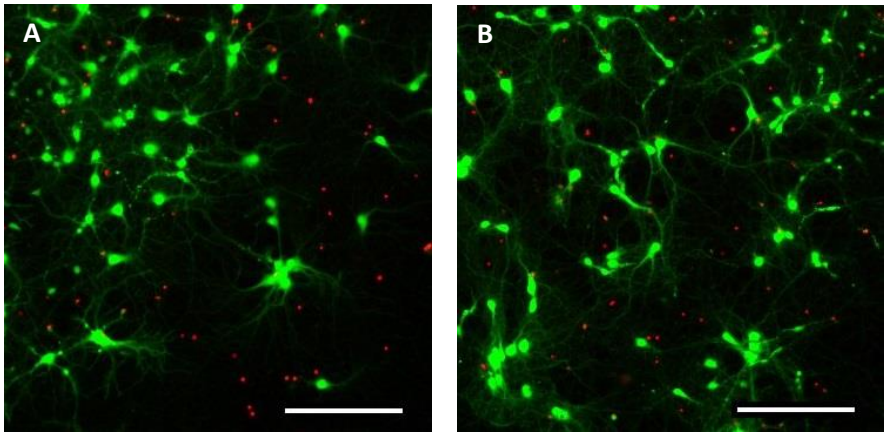

Fig. 15. CHX treatment does not lead to cell toxicity. EtOH- (A) and 1µg/ml CHX-treated (B) cells were stained with fluorescent calcein dye but not with propidium iodide, which suggests cell viability. Scale bars, 200µm.

New synthesis of βIV-Spectrin and 186-kDa Neurofascin is necessary for AIS plasticity

To perform a more specific approach, we decided to target specific long-lived AIS proteins like βIV-Spectrin and NF [18]. To do so, these genes were silenced in hippocampal neurons using shRNA at DIV 7, when the AIS is already assembled [16, 19]. Two days later (DIV 9), NaCl or KCl were added to provide baseline or chronic depolarization conditions, respectively, for 48h. With this approach, AIS plasticity was induced without some of its specific components, allowing us to understand whether AIS relocation is made by moving the previously assembled AIS complex or by assembling *de novo* in a new location.

At the day of shRNA transfection (DIV 7), as expected, most cells had mature AISs containing βIV-Spectrin, AnkG and NF (fig. 16). As such, the knock-down of specific AIS components was performed at a time point when the AIS was already assembled, not affecting its formation.

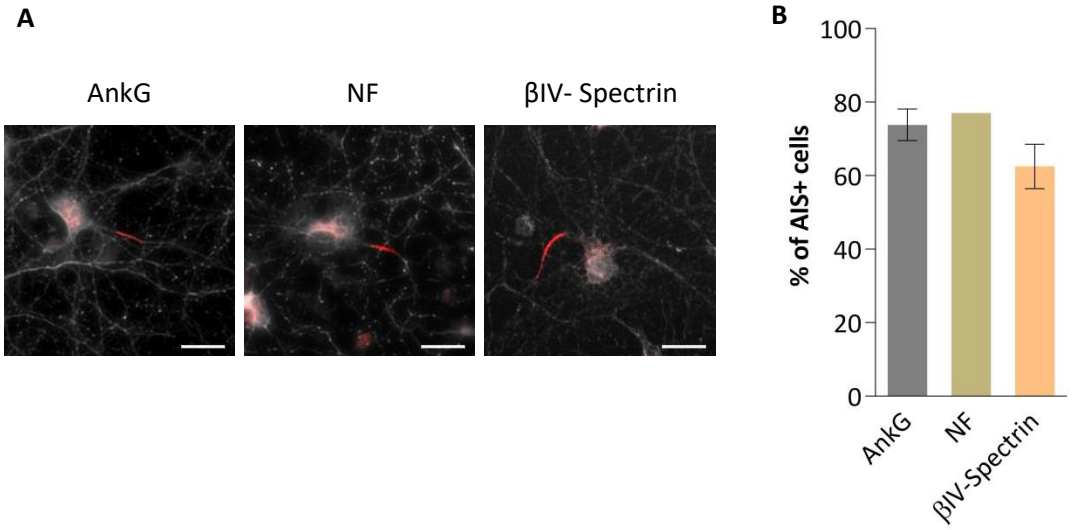

Fig. 16. The AIS is assembled at DIV7. (A) Representative images of hippocampal neurons at DIV 7, before transfection with shRNA. Cells were labeled for βIII-tubulin (white) to mark neurons, and AnkG, NF or βIV-Spectrin (red). Scale bars, 20µm. (B) Percentage of cells with AIS immunostained with AnkG, βIV-Spectrin or NF at DIV 7**.**

Control transfected cells did not show alterations in the maintenance of AnkG, NF or βIV-Spectrin at the AIS, both at baseline and after depolarization, as the transfected cells presented AISs similar to non-transfected cells (Fig. 17, 18). The knock-down of NF led to the elimination of NF from the AIS without affecting the presence of AnkG and βIV-Spectrin. This result was observed in baseline and depolarization conditions (Fig. 17, 18), suggesting that NF synthesis is necessary for its maintenance and relocation. Interestingly, the knock-down of βIV-Spectrin led to a broader effect, disrupting the AIS. Besides the elimination of βIV-Spectrin from the AIS, it also resulted in the elimination of AnkG and NF. Again, this result was observed in baseline and chronic depolarization conditions (Fig, 17, 18). These results indicate that βIV-Spectrin may play a central role in AIS maintenance, as its removal results in AIS breakdown.

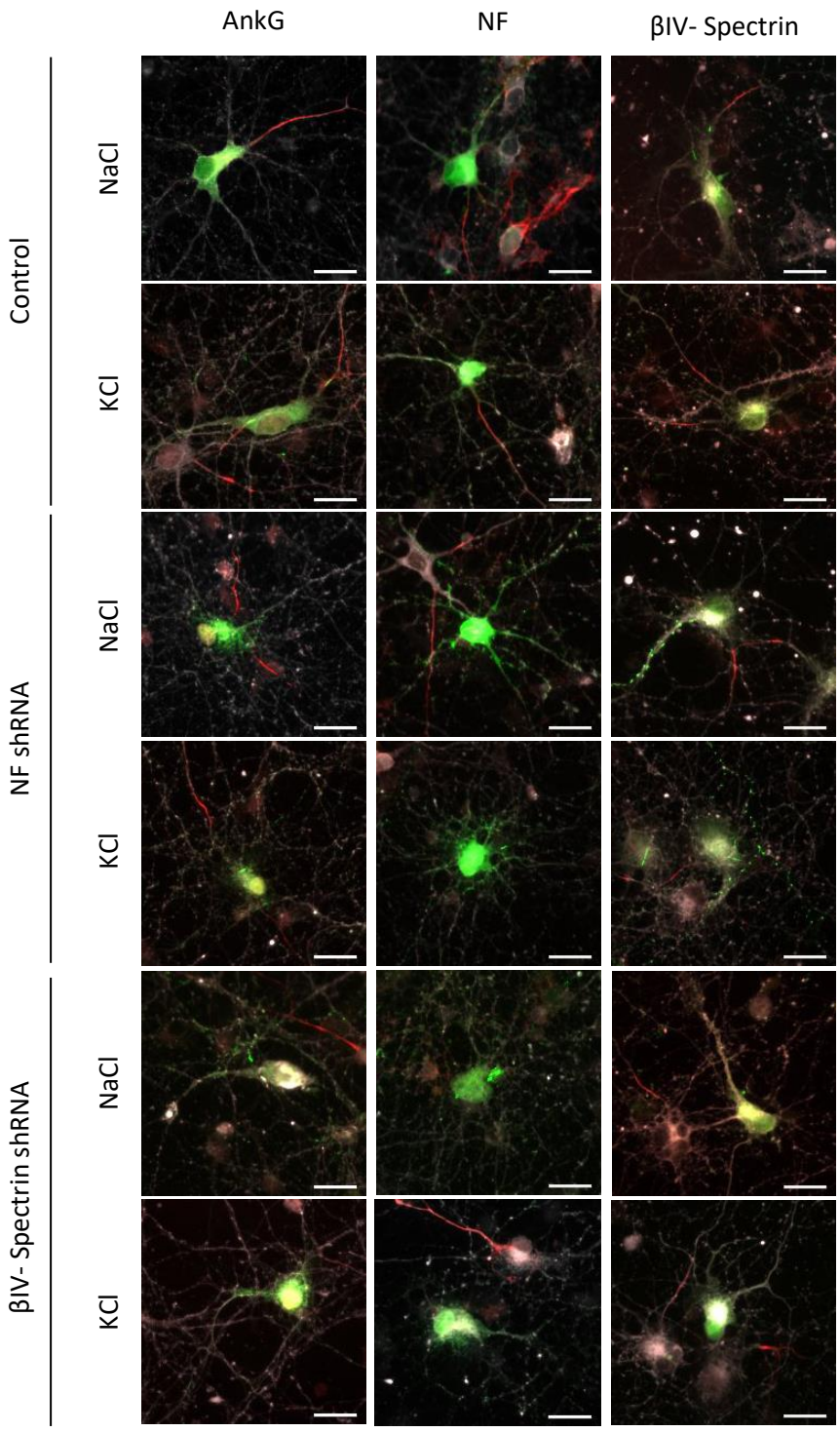

Fig. 17. NF and βIV-Spectrin are needed for AIS maintenance. Representative images of cultured hippocampal neurons transfected with control, NF shRNA or βIV-Spectrin shRNA expression plasmids and then treated with NaCl or KCl. Cells were immunostained for AnkG, NF or βIV-Spectrin (red), and βIII-tubulin (white) to mark neurons. GFP fluorescence indicates transfected cells (green). Scale bars, 20μm.

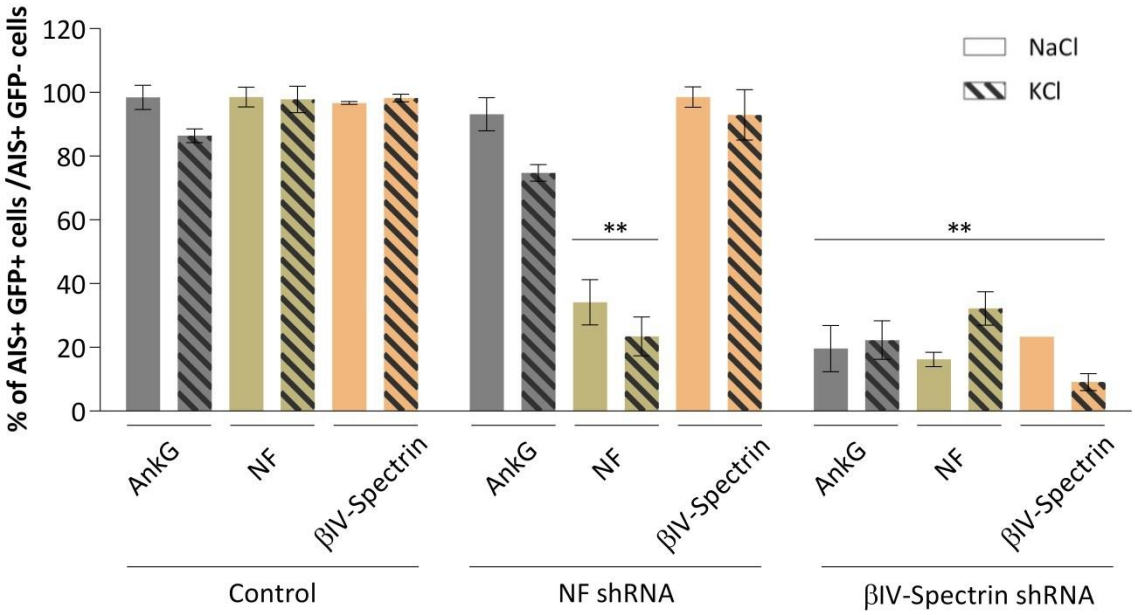

Fig. 18. New synthesis of βIV-Spectrin and 186-kDa Neurofascin is necessary for AIS plasticity. Bars indicate the normalized percentage of AIS+ transfected neurons compared to non-transfected cells. The knock-down of NF led to its elimination from the AIS, while βIV-Spectrin knock-down led not only to its elimination but also to the disappearance of AnkG and NF from the AIS. **p<0.01 compared with the respective control.

IV. Discussion

In this study we show that protein synthesis is needed for the maintenance and relocation of the AIS. The use of a broad protein synthesis inhibitor (CHX) promoted the disassembly of the AIS stochastically. Following CHX treatment, we observed AnkG clustering at the AIS of most neurons, but its mean fluorescence decreased to ~60%. Accordingly, Hedstrom *et al*. (2008) showed that four days after AnkG silencing this protein was still detectable at the AIS of most neurons, but its fluorescence intensity decreased approximately 50% compared with controls [18]. In many hippocampal neuronal subpopulations, both the beginning and end AIS positions move distally at chronic depolarization. However, in other hippocampal neuronal subtypes, such as GABAergic neurons, only the beginning AIS position suffers a distal shift [45]. There are even neuronal subtypes that show inverted plasticity, with the AIS moving proximally after treatment with high concentration of potassium [46]. In our experiments, at control conditions only the start of the AIS relocated. Nevertheless, considering the reasons pointed above, we suppose that AIS relocation occurred in control cells at chronic stimulation conditions. In contrast, CHX treatment prevented the relocation of the AIS, which suggests that protein synthesis is needed for AIS movement. However, by using CHX we prevented the synthesis of all AIS components, including AnkG. We cannot exclude that most of the observed effects in CHX treated cells are mainly due to the blockage of AnkG synthesis.

The usage of protein synthesis inhibitors is rather unspecific. To address whether the synthesis of specific AIS components is needed for AIS relocation, we performed gene silencing of AIS proteins NF and βIV-Spectrin. These AIS proteins were chosen for silencing because they were shown to be remarkably long-lived [18]. At DIV 7 most neurons have βIV-Spectrin, NF and AnkG clustered at the AIS, as shown by us and other authors [16, 19]. By knocking-down these proteins after AIS formation, we were able to address whether the AIS can re-use its components for relocation or needs newly synthetized proteins. Our results indicate that βIV-Spectrin and NF are short-lived proteins at the AIS, since gene silencing caused the loss of the respective molecule from the AIS of most neurons only four days after its knock-down. These results are the opposite

of current paradigm that with the exception of AnkG, other AIS components, including NF and βIV-Spectrin, are stable proteins with long half-lives of at least 2 weeks [18]. The stronger phenotype observed in our experiments may be explained by higher knock-down efficiencies. Although we use the same shRNA constructs, our transfection approaches are different (calcium phosphate in our case, lipofectamine in [18]). The less robust phenotype observed in [18] could result from a less efficient knock-down, allowing some gene expression that could still supply AIS maintenance.

The AIS is more dynamic than initially expected. Indeed, it was shown that just 3 hours of depolarization lead to AIS shortening [140]. These observations fit well with our results, as more labile components could explain how in a short amount of time the AIS structure can be modulated to different excitabilities.

To our knowledge, the contribution of NF and βIV-Spectrin specifically for AIS maintenance was never demonstrated before. In our work, NF knock-down did not affect the presence of other AIS components, meaning that NF is not an essential component for AIS maintenance. However, the knock-down of βIV-Spectrin resulted in AIS disassembly, as AnkG and NF were also lost. As so, besides being short-lived, βIV-Spectrin is also important for the maintenance of other proteins in the AIS. Importantly, regarding AIS molecular assembly, it is known that AnkG recruits all other AIS proteins, including βIV-Spectrin, to the AIS [13, 19, 32]. Conversely, βIV-Spectrin by itself cannot recruit AIS molecules, including AnkG [13, 19]. However, it has been proposed that besides AnkG, βIV-Spectrin may also be essential for AIS organization as βIV-Spectrin-null mice do not present AnkG or Nav channels clustered at the AIS [25]. In contrast, it was recently proposed *in vitro* that besides being long-lived, βIV-Spectrin is not essential for AIS formation or maintenance, as βIV-Spectrin shRNA transfected hippocampal neurons formed an AIS structure containing βIV-Spectrin and AnkG [19]. This *in vitro* approach may present a less severe phenotype if the shRNA is not able to eliminate βIV-Spectrin effectively, while on the βIV-Spectrin-null mice they completely lack the protein, explaining the more severe phenotype.

The nanostructure of the AIS has been recently described. βIV-Spectrin is distributed longitudinally between the subcortical actin rings forming a periodic submembrane complex at the AIS, and AnkG is associates with the periodic lattice by binding to βIV-Spectrin [23]. This model fits perfectly with our data that shows that βIV-Spectrin is a master-stabilizing factor of the AIS. βIV-Spectrin loss could lead to AnkG displacement, resulting in AIS disassembly.

Here, we show that the AIS proteins are short-lived and their synthesis is needed for both AIS maintenance and relocation. This dynamism seems to be more consistent with the plasticity of

the AIS in response to modulation of external stimuli. NF is not needed for the retention of other AIS components, while the elimination of βIV-Spectrin leads to the disruption of the AIS, suggesting that AnkG and βIV-Spectrin are both needed to maintain the AIS structure.

CHAPTER 3

The Proximal Segment of

Dorsal Root Ganglion Neurons

I. Objectives

The main focus of this work was to understand the contribution of the PS to DRG neuron polarity and to central-peripheral asymmetry. The following specific objectives were covered:

- Develop an *in vitro* model of pseudo-unipolar DRG neurons containing PS;
- Characterize the composition of the proximal segment *in vitro* and *in vivo*;
- Determine *in vivo* the ultrastructure of the stem process and peripheral and central axonal branches.

II. Methods

Embryonic DRG Neurons Culture

DRGs were dissected from E16 Wistar rat embryos. Pregnant females were euthanized and the embryos collected as previously described. For the dissection of DRGs, first, the spinal column is isolated. For that, the embryo is laid in dorsal recumbency and the skin is sprayed with 70% ethanol. An incision is made through the skin and abdominal wall muscles and continued longitudinally to the spinal column in both directions. Muscle, fat, and other soft tissues are cut from the spinal column using scissors, and then the spinal column is opened with a forcep in the midline. The extraction of DRGs is performed under a dissection microscope with a pair of forceps. Spinal ganglia are stored in ice-cold Neurobasal medium (Invitrogen) until further processing.

DRGs were digested with 0.04% Trypsin-EDTA (Invitrogen) for 1 hour at 37°C. After enzyme treatment, the digestion was stopped with 10% FBS in Neurobasal. Tissue was centrifuged at 200g for 10 min. The medium was removed and tissue resuspended in final medium (Neurobasal medium containing 2% B27 (Invitrogen), 2 mM l-glutamine (Invitrogen), 1% P/S, and 50ng/ml of nerve growth factor (Millipore)). A single cell suspension was obtained by pipetting 30 times with P1000. Cells were seeded in 24-well plates with glass coverslides coated with poly-L-lysine (20µg/mL, Sigma-Aldrich) and laminin (5µg/mL, Sigma-Aldrich), at a density of 15,000 cells per well. Cells were maintained at 37°C in final medium. The medium was partially changed two times a week.

To obtain monocultures growing in the near-absence of glial cells, 1 day after cell seeding, cells were exposed for 24 hours to the cytostatic agents uridine and 5-fluoro-2'-deoxyuridine (40 µM each, Sigma–Aldrich).

Post-natal DRG Neurons Culture

DRGs were collected from either postnatal day (P) 1.5 Wistar rats, or P1.5 and P12 Thy1-YFP-16 transgenic mice (that expresses YFP in more than 80% of DRG of neurons [141]). Postnatal rats or mice were euthanized by decapitation using scissors. The animal was laid in ventral

recumbency and the skin was sprayed with 70% ethanol. The spinal column was isolated and cut dorsal and ventrally with a scissor, cutting the dorsal column in equal halves. The spinal column hemi-segments were secured medial side up. First, the spinal cord and meninges were removed, and then individual ganglia were carefully isolated by clasping and lifting with forceps. The spinal ganglia were stored in ice-cold Neurobasal medium (Invitrogen) until further processing.

DRGs were digested with 0.125% collagenase type IV (from *Clostridium histolyticum*, Sigma-Aldrich) in DMEM/F12 (Sigma-Aldrich) with 9% FBS and 0.9% P/S for 1 hour at 37°C. After enzyme treatment, spinal ganglia are washed three times with DMEM/F12. The medium was substituted by DMEM/F12 with 10% FBS and 1% P/S and dissociation was performed by using fire-polished Pasteur pipettes. Then, cells were centrifuged at 200g for 10 min and resuspended in final medium (as described in the embryonic DRG neuron cultures). Cells were seeded and maintained as described above.

Non-contact co-cultures were established by using inserts (1µm polyester membrane, 24-well plate; BD Falcon). Inserts and wells containing coverslides were coated with poly-L-lysine and laminin as described above. 8,000 and 15,000 P1.5 Wistar rat cells were plated onto inserts and wells, respectively. At DIV 1, the cells seeded on coverslides were exposed for 24h to cytostatic agents as described above, and then the inserts were placed onto these wells.

For cell alignment studies, P1.5 Wistar rat cells were seeded on patterned microgrooved surfaces placed inside wells of 24-well plates. These surfaces consisted of a polydimethylsiloxane (PDMS) substrate patterned with microgrooves that were parallel, separated by a distance of 15µm, and had 3µm of depth and 10µm of width.

Immunocytochemistry

Previously fixed cells were incubated with 0.1% Triton-X100 (Sigma-Aldrich) in PBS for 5 min, followed by incubation with 200mM Ammonium Chloride for 10 min. Cells were washed 3 times with PBS pH 7.4 after each step. Non-specific antibody-binding sites were blocked with 2% FBS (Invitrogen), 2% albumin from bovine serum (Sigma-Aldrich) and 0.2% gelatin from cold water fish (Sigma-Aldrich) in PBS for 1 hour at room temperature, and then cells were incubated with primary antibodies diluted in blocking solution overnight at 4ºC (table 2). After three washes with PBS, cells were further incubated with the appropriate secondary antibodies for 1 hour at room temperature. Cells were washed with PBS, the slides were mounted with Fluoroshield containing DAPI (Sigma-Aldrich) and visualized under a fluorescence microscope (Leica DMI6000 B) with a

40x, 0.60 NA objective coupled to a camera (Hamamatsu C11440-22C). ImageJ was used to analyze the images and determine neuronal morphology and PS presence.

Table 2 – Primary and Secondary Antibodies used in Immunocytochemistry

	Antigen	Type	Host	Dilution	Company [Catalogue Nr.]
Primary Antibodies	AnkG	Monoclonal	Mouse	1:100	Santa Cruz Biotechnology [sc-12719]
	βIII-Tubulin	Polyclonal	Rabbit	1:500	Synaptic Systems [302302]
Secondary Antibodies	Mouse IgG	AlexaFluor®594	Donkey	1:500	Jackson ImmunoResearch Laboratories [715-585-150]
	Mouse IgG	AlexaFluor®488	Goat	1:500	Jackson ImmunoResearch Laboratories [115-545-003]
	Rabbit IgG	AlexaFluor®647	Donkey	1:200	Life technologies [A31573]
	Rabbit IgG	AlexaFluor®568	Donkey	1:500	Life Technologies [A10042]

DRG Immunohistochemistry

DRGs were collected from 16 week-old Wistar rats and fixed in 2% PFA for 2 hr at 4°C. Tissues were then washed once with PBS and incubated in 20% sucrose in PBS, overnight at 4°C. Thirty µm free floating cryosections were cut and then incubated in methanol for 20 min. Sections were washed with water and the fluorescence quenched with 0.1% sodium borohydride (sigma-Aldrich) followed by 200mM ammonium chloride. Sections were incubated with immunoglobulin blocking agent (vector) for 45 min at room temperature, blocked with 0.5% fish gelatin in PBS at 37°C for 1 hr and then incubated with primary antibodies (anti-AnkG, 1:1000 in blocking buffer, Neuromab 75-146; βIII-tubulin, 1:150, St John's Laboratory STJ97123) overnight at 4°C. On the next days, sections were washed with PBS and incubated with secondary antibody (anti-mouse AlexaFluor®594, 1:500, Jackson ImmunoResearch Laboratories 715-585-150; anti-rabbit AlexaFluor®488, 1:500, Invitrogen A21206). Sections were washed, placed in a slide, air dried and mounted with fluoroshield (Sigma-Aldrich). Images were taken with a fluorescence microscope (Zeiss Axio Imager Z1) with a 40x oil objective coupled to a camera (Axiocam MR ver. 3.0).

Correlative light and electron microscopy

DRGs were dissected from 6 week-old Thy1-EGFP-M transgenic mice. These mice express GFP in less than 10% of all DRG neurons [141]. Tissues were fixed for 2 hours in 2.5% glutaraldehyde (GTA, Polysciences) and 2% PFA in PBS, followed by incubation overnight at 4°C in PBS. DRGs were embedded in 1.5% agar (Sigma-Aldrich) and 200-µm-thick sections were cut using

a vibrotome (Leica VT1000S). Agar sections containing dorsal root ganglia were stored in PBS, at 4°C until further use. The agar sections were visualized using a fluorescence microscope (Zeiss AxioImager Z1) to identify the spinal ganglia that have fluorescent neurons with visible stem process and/or T-junction. The sections of agar containing these ganglia were stored back in PBS, at 4°C.

To mark the regions of interest, a two-photon microscope was used according to the near-infrared branding (NIRB) technique [142]. In collaboration with Dr. Gabriel Martins from Instituto Gulbenkian de Ciência, the multi-photon Zeiss STereo LUMAR stereoscope was used. Selected sections were visualized and either the stem process or the T-junction marked with two-photon laser by drawing a square around the region of interest. The size of NIRB marks was regulated by modulating laser power and exposure time. The precise relationship between laser dose and mark size depended on the *z*-depth of a mark, as tissue attenuates the laser. To generate NIRB marks, the laser was tuned to λ = 850 nm and its power was set between 100 and 200 mW in the back focal plane. Typically, a pixel dwell time of 70 µs was used and, for each area of interest, several series were performed under visual control until appearance of red autofluorescence.

The marked sections were then stored in 0.1M sodium cacodylate (Delta Microscopies) and then processed for electron microscopy. Briefly, the tissue was post fixed with 1% osmium tetroxide with 1.5% potassium ferricyanide for 1hr. Following 3 washes with 0.1M sodium cacodylate buffer the samples were dehydrated in increasing ethanol solutions followed by propylene oxide. The samples were resin (Araldite with Epon) embedded 48 hr after incubation at 65°C. One µm semi-thin sections were performed until the marks are present. Then, 50 nm ultra-thin sections were cut and analyzed by electron microscopy.

Statistical Analysis

All values are presented as mean±SEM. Statistical analysis was performed using GraphPad Software. Significance was determined using Two-way ANOVA.

III. Results

DRG neurons develop a pseudo-unipolar morphology with a proximal segment *in vitro*

To establish an *in vitro* model of pseudo-unipolar DRG neurons containing PS, several independent cell cultures were performed with neonatal Thy1-YFP-16 transgenic mice and embryonic and neonatal Wistar rats.

First, DRG neurons from P1.5 and P12 Thy1-YFP transgenic mice were cultured. Most DRG neurons of these mice express YFP under control of the neuronal promoter Thy1, thus allowing single-cell labeling [141]. These neurons were maintained in two conditions: co-cultures (with DRG neurons and glial cells) and monocultures (DRG neurons only). For both conditions, the results were similar for either P1.5 or P12 cultures. At these ages, the number of fluorescent neurons was very low and YFP fluorescence was not strong enough to allow the visualization of neuronal morphology. Moreover, even at DIV 28, these neurons did not seem to contain PS, although some AnkG clustering was found in some neurites (fig. 19). As a consequence, no further studies were performed using this mouse model.

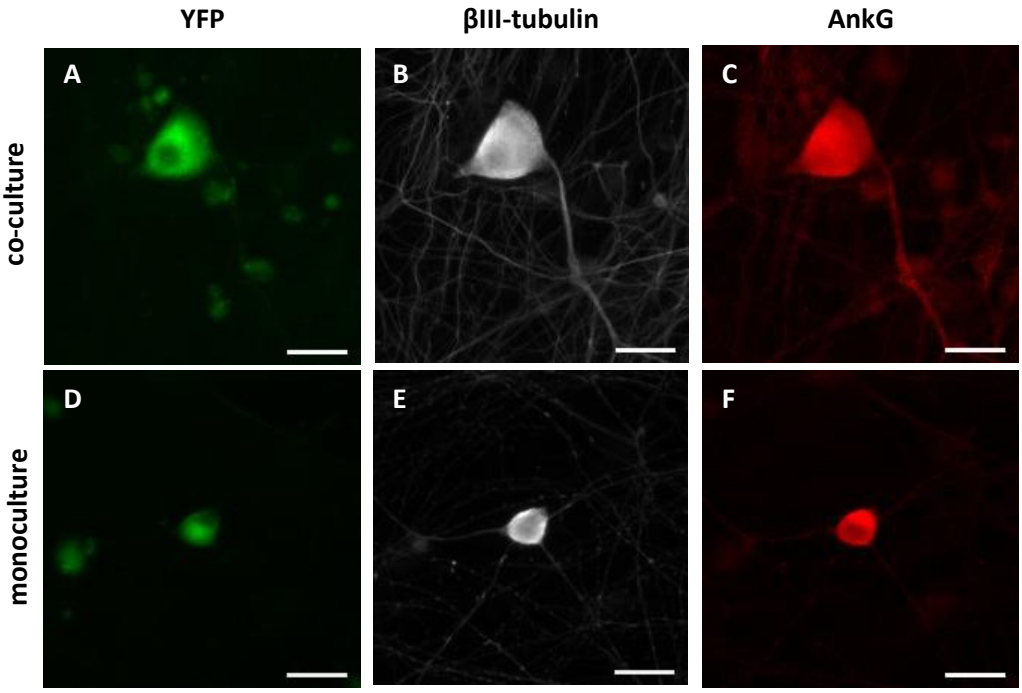

Fig. 19. Thy1-YFP-16 mice DRG neurons at DIV 28 do not possess PS. For each condition, the same region of interest is shown with representative neurons expressing yellow fluorescent protein (YFP), immunolabeled for βIII-tubulin to mark the neuronal cell body and neurites or AnkG to mark the proximal segment. Scale bars, 20µm.

Next, we performed co-cultures of DRG neurons and glial cells from E16 Wistar rat embryos. With this approach we were able to evaluate neuronal morphology, despite the absence of single-neuron labeling. Moreover, these Wistar rat DRG neurons possessed PS, as an enriched AnkG labeling was found in the initial part of their neurites (fig. 20). To evaluate neuronal morphology, we divided neurons in 3 categories: multipolar (with more than 3 processes emerging from the cell body), bell-shaped or bipolar (two processes emerging from the cell body) and pseudo-unipolar (one process emerging from the cell body). An example of each can be seen in fig. 20.

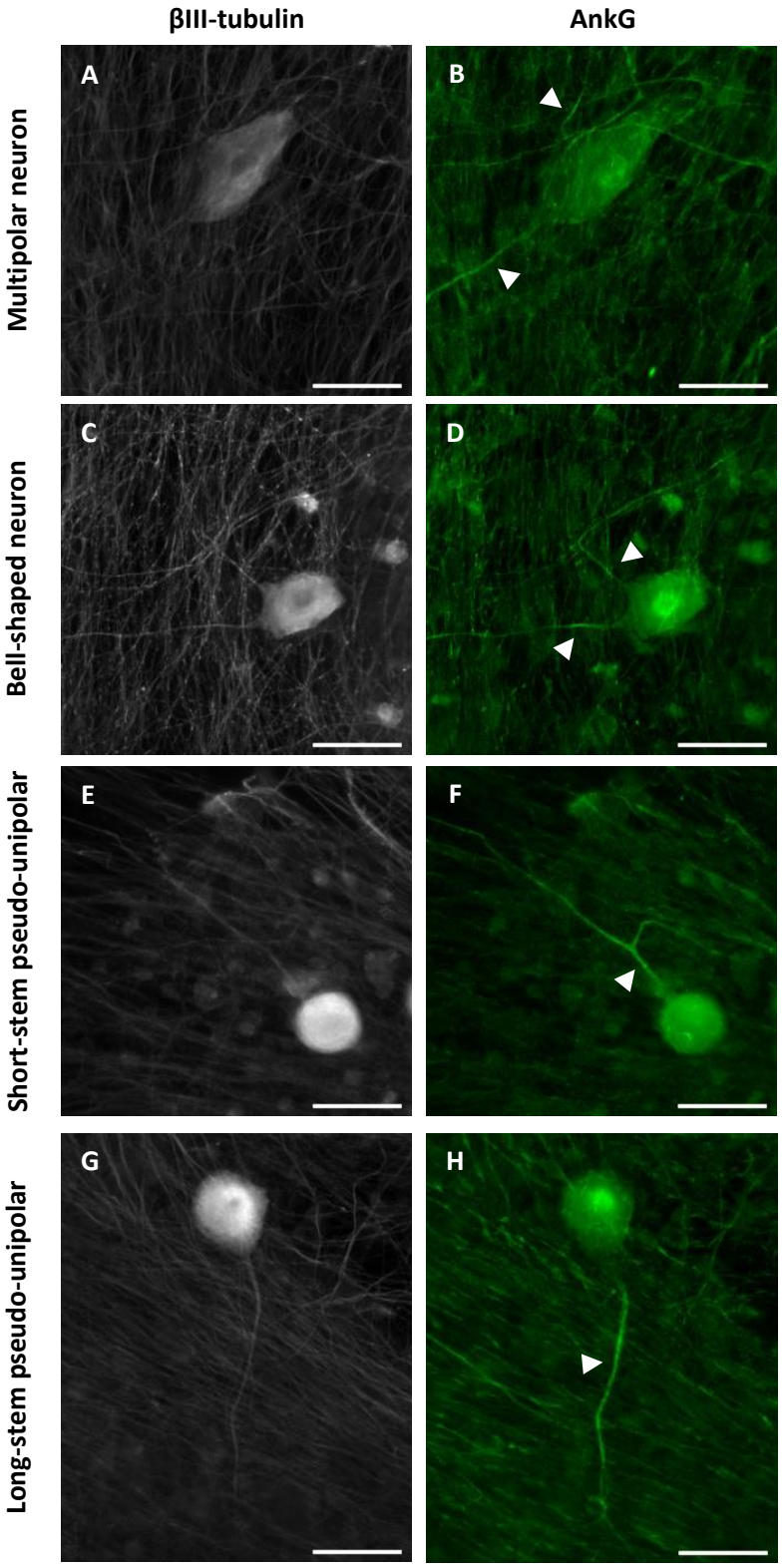

Fig. 20. *In vitro* DRG neurons develop a pseudo-unipolar morphology with a proximal segment. Representative images of multipolar, bell-shaped, short-stem pseudo-unipolar, and long-stem pseudo-unipolar neurons. For each morphological type, the same region of interest is shown with neurons

immunolabeled for βIII-tubulin to mark the neuronal cell body and neurites, or AnkG to mark the proximal segment (indicated by arrows). Scale bars, 40µm.

At DIV 7, there were already some pseudo-unipolar neurons, and their percentage increased over time, reaching 57% at DIV 28. On the contrary, the percentage of multipolar and bell-shaped neurons decreased along time (fig. 21A). The percentage of neurons possessing at least one PS also increased over time, reaching 82% at DIV 28, when most neurons possess only one PS (fig. 21B). Multipolar, bell-shaped and bipolar neurons had a variable number of PSs (ranging from none to four), while most pseudo-unipolar neurons had only one PS that could continue after neurite bifurcation (fig. 21C). Interestingly, we noticed that almost all neurons with a stem process smaller than 60µm had a PS that continued beyond the bifurcation along both axons, while almost all neurons with a stem process larger than 60µm had a PS that ends before the bifurcation (as represented in fig. 20). As so, we defined two types of pseudo-unipolar neurons, short-stem and long-stem, according to the size of the stem process. There was not a statistical difference in the PS end or start positions between short-stem and long-stem pseudo-unipolar neurons (fig. 21D).

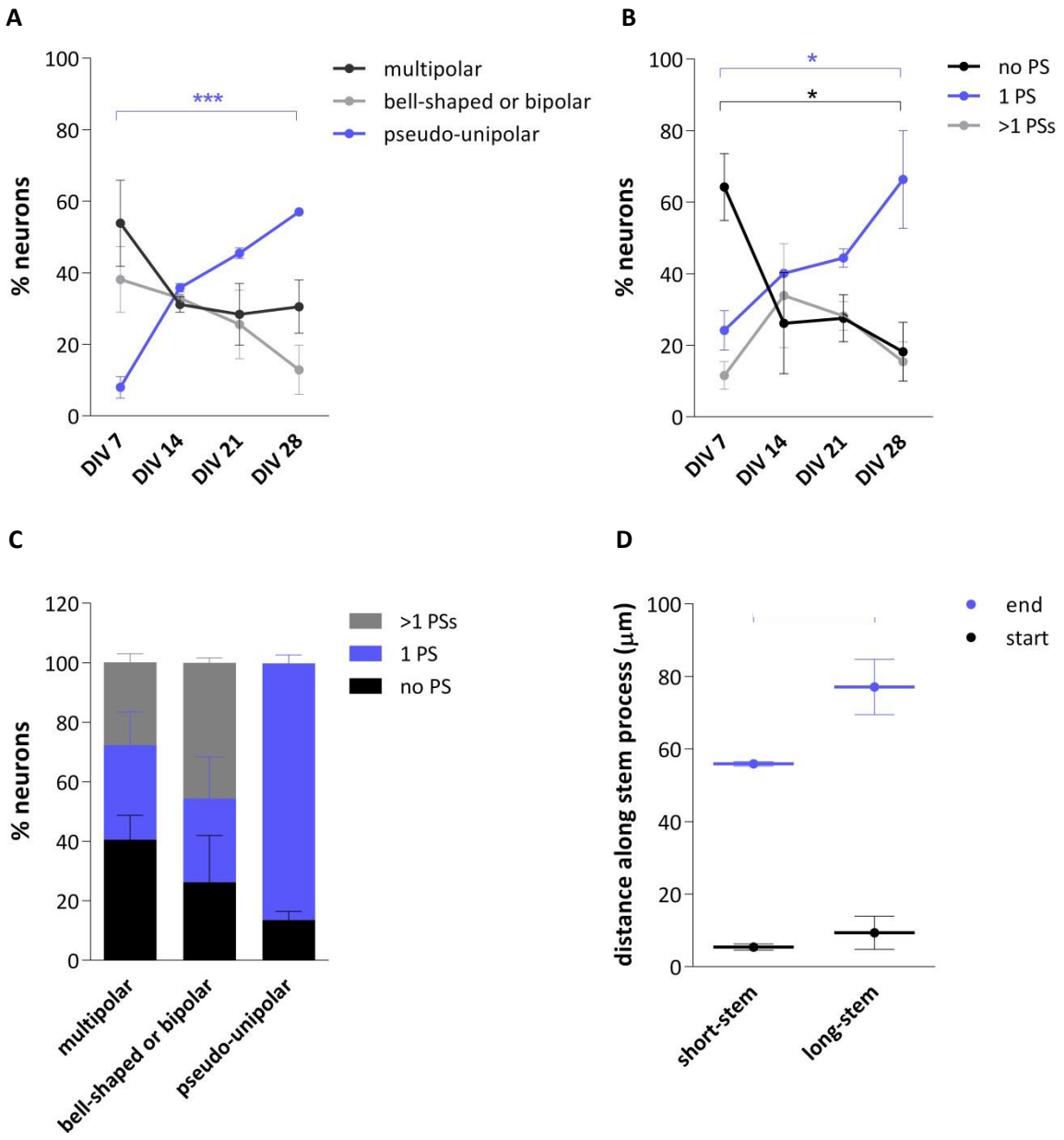

Fig. 21. DRG neurons from E16 Wistar Rats polarize when in co-culture. (A) Morphological analysis of DRG neurons showing the percentage of neurons possessing multipolar, bell-shaped or bipolar, and pseudo-unipolar morphology, at each time point. (B) Percentage of neurons having none, one or more PSs, at different times in culture. (C) Percentage of neurons having none, one or more PSs for each morphological type considering neurons from DIV 21 and 28. (D) Start and end positions of the PS of short-stem and long-stem pseudo-unipolar neurons, at DIV 28. *p<0.05, ***p<0.001.

Contact with non-neuronal cells is necessary for pseudo-unipolarization and PS formation

The AIS is established from an intrinsic property of multipolar neurons [15]. To determine if the PS of DRG neurons is also intrinsically determined or if the glial cells play a role, we compared its formation in co-cultures with monocultures of neurons and co-cultures in transwell systems (monoculture of DRG neurons in the bottom and glial cells on the insert). Co-cultures of DRGs from P1.5 Wistar rats were performed and the cells maintained until DIV 21. At this time point the percentage of pseudo-unipolar neurons was 35% (fig. 22A, B), slightly smaller than that of the E16 co-culture at DIV 21 (45%, fig. 21A). Similarly with the E16 co-cultures, most neurons from P1.5 co-cultures possessed at least one PS (fig. 22C). At DIV 21, monocultures of P1.5 Wistar rat DRG neurons had an appearance very different from co-culture neurons (fig. 22A). Neuronal morphology was not possible to analyze. However, it was possible to notice that PSs were completely absent (fig. 22C). Since DRG neurons only present a PS when co-cultured with glial cells, we decided to culture DRG neurons using a transwell system to assess the role of soluble factors on pseudo-unipolarization and PS formation. At DIV 21, transwell co-cultures presented a general appearance that resembled the co-culture (fig. 22A). However, neuronal morphology was quite different, since in transwell co-cultures 87% of neurons presented multipolar morphology and 91% of neurons did not have PS (fig. 22B,C). It is important to mention that we verified by DAPI staining that there were some non-neuronal cells contacting neurons (results not shown). Overall, these results suggest that pseudo-unipolarization and PS assembly require contact with glial cells, since the transwell system did not significantly improve neuronal morphology and PS formation.

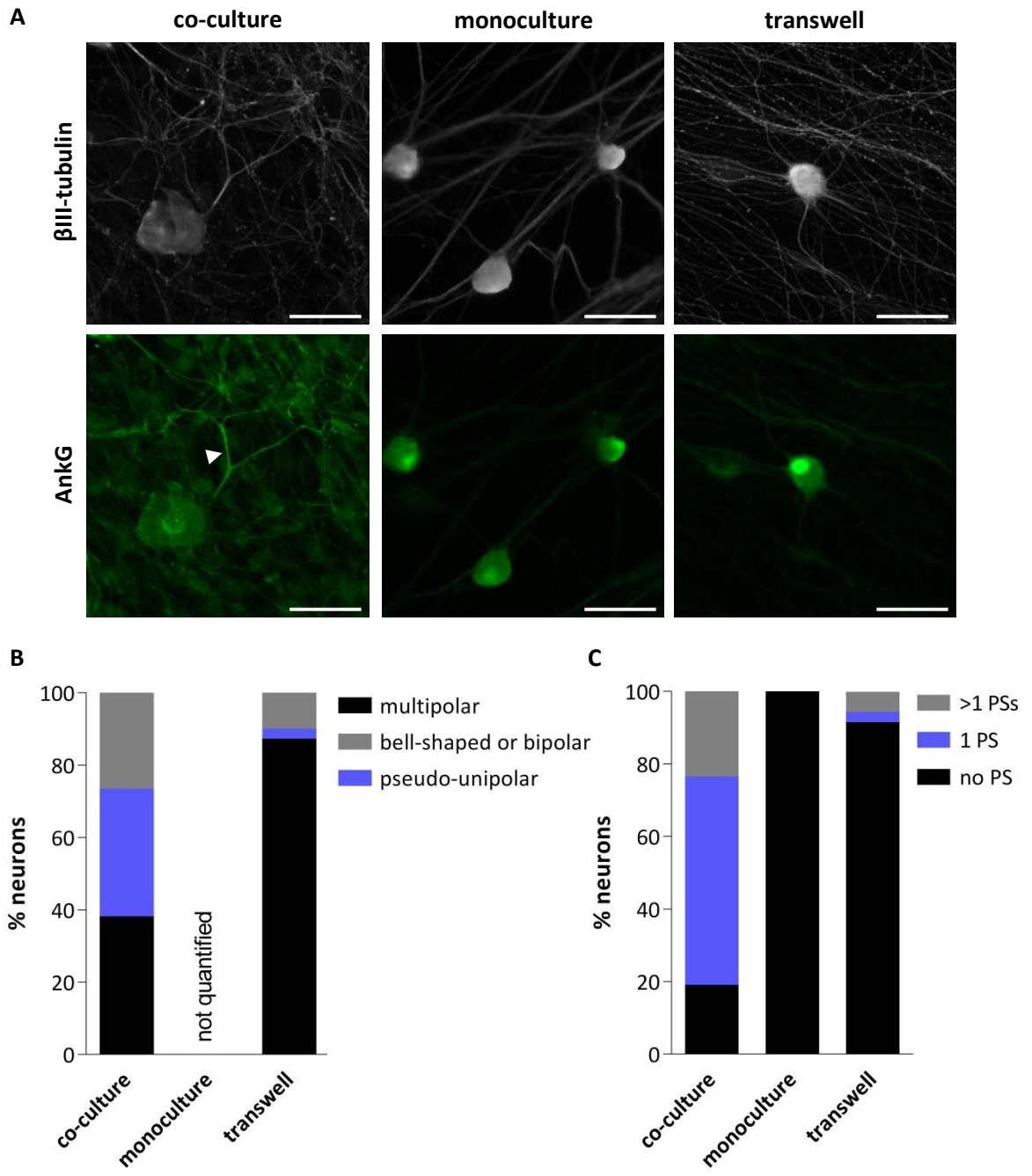

Fig. 22. Contact with non-neuronal cells is necessary for pseudo-unipolarization and PS formation. (A) Representative images of DRG neurons in co-culture, monoculture, and in transwell systems, at DIV 21. Neurons are immunolabeled with βIII-tubulin (grey) to mark the neuronal cell body and neurites, and with AnkG (green) to mark the PS (indicated by arrow). Scale bars, 40µm. (B) Graph of the percentage of neurons possessing multipolar, bell-shaped or bipolar, and pseudo-unipolar morphology. (C) Graph showing the percentage of neurons containing none, one or more than one PSs.

To assess whether pseudo-unipolarization and PS formation can be induced by topographic cues, DRG neurons from P1.5 Wistar rats were cultured on microgrooved substrates and maintained until DIV 28. DRG neurons were grown in two conditions: co-culture and non-contact co-culture using transwell plates. In both conditions, there were very few neurons on substrates, and neurites were mostly aligned with the microgrooves. However they grew both inside and outside of them. In addition, neuronal morphology was difficult to analyze. In both conditions most neurons were bipolar and no proximal segments were detected (fig. 23).

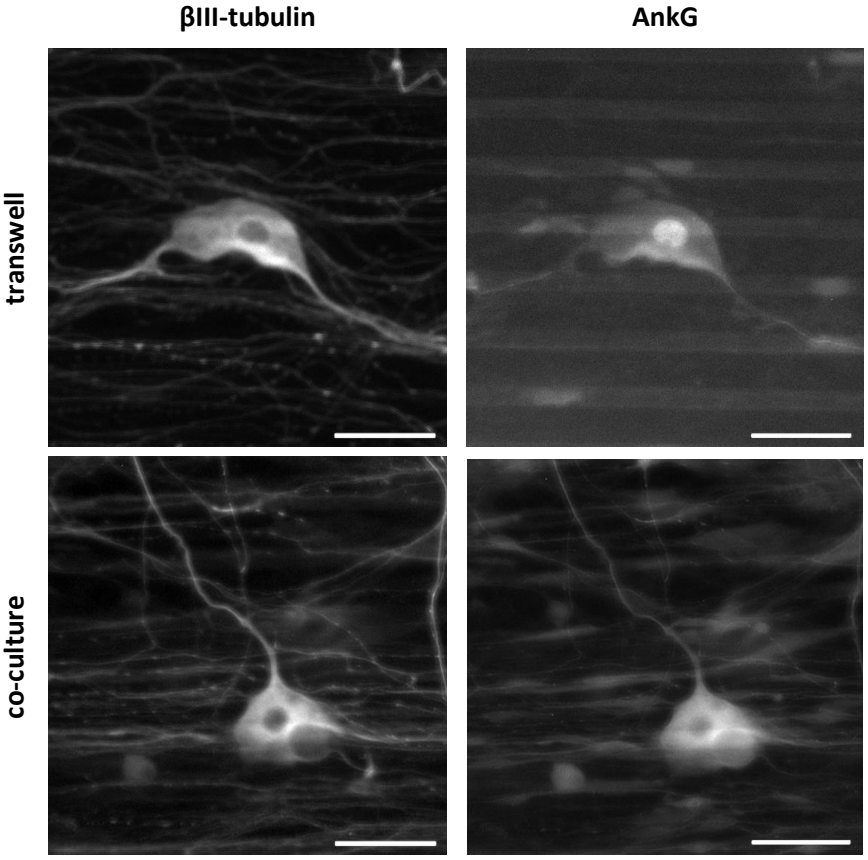

Fig. 23. Wistar rat DRG neurons cultured on microgrooved substrates do not present PS. Representative images of DRG neurons at DIV 21 in non-contact co-culture using transwell systems, and contact co-culture. For each condition, the same region of interest is shown with neurons immunolabeled for βIII-tubulin to mark the neuronal cell body and neurites, or AnkG to mark the proximal segment. Scale bars, 40µm.

Detection of the proximal segment *in vivo*

To verify the existence of the PS in vivo, we performed immunofluorescence on DRG sections of adult Wistar rats. We detected AnkG clustering corresponding to nodes of Ranvier and also in a few regions where it seemed to correspond to PSs (fig. 24A). However, when a double immnunofluorescence was performed for AnkG and βIII-tubulin, we were not able to find an AnkG clustering on a βIII-tubulin axon (fig. 24B). So far we were not able to identify the PS *in vivo* without any doubt.

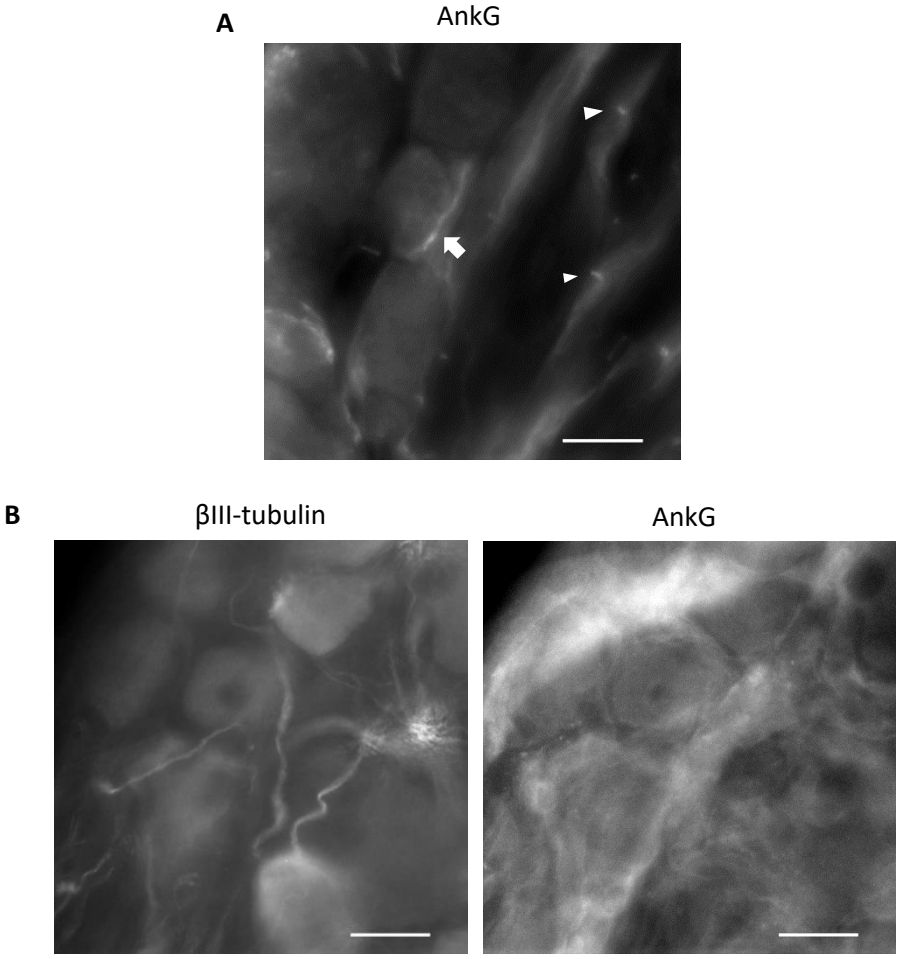

Fig. 24. Proximal segment *in vivo*. Representative images of adult Wistar rat DRG sections. (A) Z-stack image showing AnkG clustering at nodes of Ranvier (arrowheads) and seemingly at PS (arrow). (B) In βIII-tubulin axons, no AnkG staining was found. Scale bar, 20µm.

Correlative light and electron microscopy

One of our goals was to determine *in vivo* the ultrastructure of the stem process and peripheral and central axonal branches, using fluorescence coupled with electron microscopy in DRG from Thy1-EGFP-M mice. For that, we used NIRB [142] to create fiducial marks in defined three-dimensional positions in tissue fixed for electron microscopy (fig. 25A). Few 200 µm-thick agar sections of DRGs contained neurons expressing EGFP, and these were selected for the NIRB technique. We were able to create fiducial marks on the stem process and on the bifurcation of DRG neurons expressing EGFP. We also confirmed that fiducial marks were easily identified by transmitted-light images before and after processing for electron microscopy (fig. 25B).

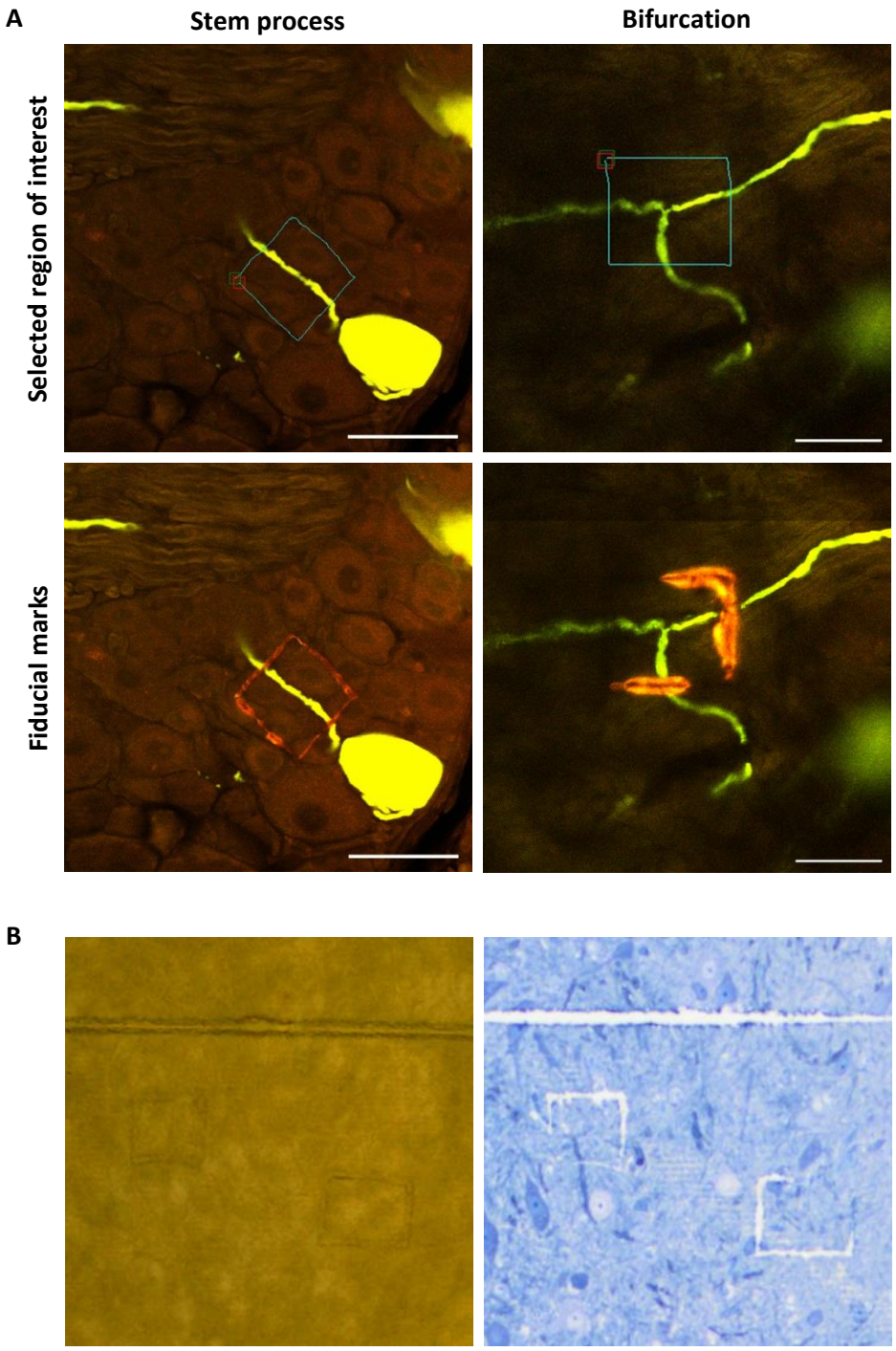

Fig. 25. Induction of fiducial marks with 2-photon microscopy. (A) Representative images showing selected regions of interest of DRG neurons expressing EGFP, before and after the induction of fiducial marks using 2-photon microscopy. Scale bars, 50µm. (B) Transmitted-light images of a spinal cord cross-section showing that fiducial marks can be easily identified both before (left, 200µm vibratome section) and after (right, 1µm semi-thin section) processing for electron microscopy.

IV. Discussion

One major goal of this work was to establish an *in vitro* model of pseudo-unipolar DRG neurons containing PS. For that, several long-term cell cultures were performed in several conditions and with cells from different origins.

Monocultures and co-cultures with neurons from postnatal Thy1-YFP-16 transgenic mice from P 1.5 and P12 were not suitable for the desired *in vitro* model. These mice were chosen as cell origin because their neurons express YFP under control of elements of the neuronal promoter Thy1, thus allowing single-cell labeling. Thy1 is a late embryonic promoter and even at P12 YFP intensity was not bright enough to have good single-cell labeling. Furthermore, we did not observe any PS on these cells suggesting that this approach is not suitable for an *in vitro* model.

By performing DRG co-cultures from embryonic (E16) and postnatal (P1.5) Wistar rats, we obtained *in vitro* systems where many neurons were pseudo-unipolar and had one PS. The embryonic co-cultures were more successful comparing to the postnatal co-cultures, since the percentage of pseudo-unipolar neurons was higher in the former ones. These results suggest that as animals grow older, DRG neurons lose their ability to recapitulate embryonic development and acquire a pseudo-unipolar morphology. Concerning the embryonic co-culture, our results show that there was neuronal maturation over time, as multipolar and bipolar neurons became pseudo-unipolar. These results suggest that similar to what happens *in vivo* [83], pseudo-unipolarization also happens *in vitro*. Other interesting feature was that we could identify two different pseudo-unipolar types of DRG neurons based on the size of the stem process that possessed a different location of the PS. Short-stem pseudo-unipolar neurons possessed a PS that continued after the bifurcation, while long-stem pseudo-unipolar neurons possessed a PS that ended before the bifurcation. Interestingly, while hippocampal neurons usually possess an AIS with ~20-40µm [13], the PS was remarkably longer (59.1±7.0 µm).

In our system, pseudo-unipolar morphology with the presence of PS was obtained successfully when DRG neurons were in contact with glial cells. Furthermore, non-contact co-

cultures had few neurons with PS and pseudo-unipolar morphology. The existence of some non-neuronal cells in the wells may allow some cell contacts enabling few cells to form a PS and acquire a pseudo-unipolar morphology. Anyway, we cannot exclude that some soluble factor may also contribute to this process. Accordingly, the requirement of non-neuronal cells for pseudo-unipolarization was reported by other authors [84, 87]. In addition, in myelinating co-cultures, the presence of PS has been reported [13, 19, 34]. In our experiments contact co-cultures were not in myelinating conditions. As such, PS formation may be dependent on non-neuronal contact but independent of myelin formation. Furthermore, our results contradict the observations of Zhang and Bennet (1998), who reported that PS formation is an intrinsic mechanism and does not require the presence of non-neuronal cells [135].

It has been shown that neuronal polarization can be manipulated with surface topography [143]. In our experiments, a small distance between grooves was chosen to assure that all neurites could encounter grooves, and a small width of grooves was chosen to guide the neurites. We observed that the microgrooved pattern used was not able to mimic the contact of non-neuronal cells as it did not promote PS formation and pseudo-unipolarization. In fact, when co-cultures were performed in the microgrooved substrate, PS formation was inhibited, although there were some pseudo-unipolar cells. In conclusion, we consider that this microgrooved pattern is not suitable to obtain the desired *in vitro* model. Other patterns may be tested to verify whether PS formation and pseudo-unipolarization could be improved.

The existence of a PS *in vivo* was not detected so far. We were not able yet to identify an AnkG rich zone in a βIII-tubulin positive stem process. The organization of the DRG make it difficult to identify the stem process, as in most cases it is located around other neurons.

Using a correlative light and electron microscopy method as reported in other studies [142], we have been able to successfully produce fiducial marks in DRG sections. Fiducial marks were not easy to see by electron microscopy. As so, a few modifications to this strategy may be needed. Nevertheless, electron microscopy analysis is being performed.

Conclusion and Future Perspectives

In multipolar neurons, the AIS represents a dynamic signal processing unit, regulating the integration of synaptic inputs and intrinsic excitability. In addition, the AIS is crucial for the maintenance of neuronal polarity. Basic neuroscience has just begun to reveal the fundamental molecular mechanisms that control AIS functioning. Disrupted AIS roles may be a common feature of many nervous system diseases and injuries, so new insights may lead to the development of novel therapeutic approaches in the future.

The AIS is regarded as a highly stable structure comprised by remarkably long-lived molecules, with the exception of AnkG. However, neurons regulate their intrinsic excitability via plastic changes in AIS length and/or location. Here we investigated the mechanism of AIS relocation in response to chronic depolarization in dissociated hippocampal neurons. We specifically aimed at understanding if the AIS relocates by assembling *de novo* or by moving the previously assembled AIS. We demonstrated that Neurofascin and βIV-Spectrin are short-lived at the AIS and their synthesis is needed for both AIS maintenance and relocation. In addition, the current paradigm is that the scaffolding protein AnkG is the key molecule required for AIS formation and maintenance. However, in this work we showed that βIV-Spectrin contributes to AIS maintenance, something which was never demonstrated before. In summary, our results challenge the current paradigm that AIS molecules are long-lived and only AnkG is short-lived and necessary for AIS maintenance. It would be interesting to determine whether other AIS components, like Nav channels and neuronal CAMs, are long-lived and/or important for AIS maintenance using a similar approach.

DRG neurons possess a peculiar morphology. *In vitro*, cultured DRG neurons possess a PS, which has a molecular composition and localization similar to the AIS. The PS is an enigmatic structure because it was never reported *in vivo*, and its eventual functions are completely unknown. In case it exists *in vivo*, it may contribute to the pseudo-unipolar morphology and/or to the central-peripheral polarity of DRG neurons. In this work we successfully developed an *in vitro* model of DRG neurons with pseudo-unipolar morphology and containing PS. This model will

certainly be useful for answering many basic questions regarding the fine structure and physiology of these neurons. In future studies, it would be interesting to determine not only the mechanism of pseudo-unipolarization but also PS formation and positioning during this morphological transition. In addition, the identification of other molecules comprising the PS will also be possible. It would also be interesting to check if there are any structural or functional differences between the two processes arising from these neurons *in vitro*. *In vivo*, it is not known what ultrastructural differences justify the strikingly different functional properties between the central and peripheral axons. Many ultrastructural studies were performed decades ago, but technical difficulties did not allow the definite determination of the fine structure of DRG neurons. As so, in this work we established a technique of correlative light and electron microscopy to analyze the fine structure of DRG neurons. In the future, this technique will be used by us to analyze the ultrastructural features of DRG neurons.

In conclusion, in this work we have expanded the knowledge about AIS plasticity and have established an *in vitro* model and techniques that will be useful for future studies with DRG neurons.

References

1. Siegel, A. and H.N. Sapru, *Essential Neuroscience*. 2010: Wolters Kluwer Health/Lippincott Williams & Wilkins.

2. Lodish, H.F., *Molecular Cell Biology 6 Ed*. 2008: W. H. Freeman and Company.

3. Hammond, C., *Cellular and Molecular Neurophysiology*. 2014: Elsevier Science.

4. Ramírez, O.A. and A. Couve, *The endoplasmic reticulum and protein trafficking in dendrites and axons.* Trends in Cell Biology, 2011. **21**(4): p. 219-227.

5. Debanne, D., et al., *Axon physiology.* Physiol Rev, 2011. **91**(2): p. 555-602.

6. Merianda, T.T., et al., *A functional equivalent of endoplasmic reticulum and Golgi in axons for secretion of locally synthesized proteins.* Molecular and cellular neurosciences, 2009. **40**(2): p. 128-142.

7. Koenig, E., et al., *Cryptic peripheral ribosomal domains distributed intermittently along mammalian myelinated axons.* J Neurosci, 2000. **20**(22): p. 8390-400.

8. Amerman, E.C., *Human Anatomy & Physiology*. 2015: Pearson Education.

9. Barnes, A.P. and F. Polleux, *Establishment of axon-dendrite polarity in developing neurons.* Annu Rev Neurosci, 2009. **32**: p. 347-81.

10. Conde, C. and A. Caceres, *Microtubule assembly, organization and dynamics in axons and dendrites.* Nat Rev Neurosci, 2009. **10**(5): p. 319-332.

11. Tahirovic, S. and F. Bradke, *Neuronal Polarity.* Cold Spring Harbor Perspectives in Biology, 2009. **1**(3): p. a001644.

12. Dotti, C.G., C.A. Sullivan, and G.A. Banker, *The establishment of polarity by hippocampal neurons in culture.* J Neurosci, 1988. **8**(4): p. 1454-68.

13. Yang, Y., et al., *βIV spectrin is recruited to axon initial segments and nodes of Ranvier by ankyrinG.* The Journal of Cell Biology, 2007. **176**(4): p. 509-519.

14. Szu-Yu Ho, T. and M.N. Rasband, *Maintenance of neuronal polarity.* Dev Neurobiol, 2011. **71**(6): p. 474-82.

15. Ogawa, Y. and M.N. Rasband, *The functional organization and assembly of the axon initial segment.* Curr Opin Neurobiol, 2008. **18**(3): p. 307-13.

16. Boiko, T., et al., *Ankyrin-dependent and -independent mechanisms orchestrate axonal compartmentalization of L1 family members neurofascin and L1/neuron-glia cell adhesion molecule.* J Neurosci, 2007. **27**(3): p. 590-603.

17. Grubb, M.S. and J. Burrone, *Building and maintaining the axon initial segment.* Current opinion in neurobiology, 2010. **20**(4): p. 481-488.

18. Hedstrom, K.L., Y. Ogawa, and M.N. Rasband, *AnkyrinG is required for maintenance of the axon initial segment and neuronal polarity.* The Journal of Cell Biology, 2008. **183**(4): p. 635-640.

19. Hedstrom, K.L., et al., *Neurofascin assembles a specialized extracellular matrix at the axon initial segment.* The Journal of Cell Biology, 2007. **178**(5): p. 875-886.

20. Galiano, M.R., et al., *A distal axonal cytoskeleton forms an intra-axonal boundary that controls axon initial segment assembly.* Cell, 2012. **149**(5): p. 1125-39.

21. D'Este, E., et al., *STED Nanoscopy Reveals the Ubiquity of Subcortical Cytoskeleton Periodicity in Living Neurons.* Cell Reports, 2015. **10**(8): p. 1246-1251.

22. Xu, K., G. Zhong, and X. Zhuang, *Actin, spectrin and associated proteins form a periodic cytoskeletal structure in axons.* Science (New York, N.Y.), 2013. **339**(6118): p. 10.1126/science.1232251.

23. Leterrier, C., et al., *Nanoscale Architecture of the Axon Initial Segment Reveals an Organized and Robust Scaffold.* Cell Reports, 2015. **13**(12): p. 2781-2793.

24. Lacas-Gervais, S., et al., *βIVΣ1 spectrin stabilizes the nodes of Ranvier and axon initial segments.* The Journal of Cell Biology, 2004. **166**(7): p. 983-990.

25. Komada, M. and P. Soriano, *βIV-spectrin regulates sodium channel clustering through ankyrin-G at axon initial segments and nodes of Ranvier.* The Journal of Cell Biology, 2002. **156**(2): p. 337-348.

26. Jones, S.L., F. Korobova, and T. Svitkina, *Axon initial segment cytoskeleton comprises a multiprotein submembranous coat containing sparse actin filaments.* J Cell Biol, 2014. **205**(1): p. 67-81.

27. Kapitein, Lukas C. and Casper C. Hoogenraad, *Building the Neuronal Microtubule Cytoskeleton.* Neuron, 2015. **87**(3): p. 492-506.

28. Leterrier, C., et al., *End-binding proteins EB3 and EB1 link microtubules to ankyrin G in the axon initial segment.* Proc Natl Acad Sci U S A, 2011. **108**(21): p. 8826-31.

29. Buffington, S.A. and M.N. Rasband, *The axon initial segment in nervous system disease and injury.* The European journal of neuroscience, 2011. **34**(10): p. 1609-1619.

30. Yoshimura, T. and M.N. Rasband, *Axon initial segments: diverse and dynamic neuronal compartments.* Current opinion in neurobiology, 2014. **0**: p. 96-102.

31. Bender, K.J. and L.O. Trussell, *The physiology of the axon initial segment.* Annu Rev Neurosci, 2012. **35**: p. 249-65.

32. Pan, Z., et al., *A common ankyrin-G-based mechanism retains KCNQ and NaV channels at electrically active domains of the axon.* J Neurosci, 2006. **26**(10): p. 2599-613.

33. Rasband, M.N., *Composition, assembly, and maintenance of excitable membrane domains in myelinated axons.* Seminars in cell & developmental biology, 2011. **22**(2): p. 178-184.

34. Dzhashiashvili, Y., et al., *Nodes of Ranvier and axon initial segments are ankyrin G–dependent domains that assemble by distinct mechanisms.* The Journal of Cell Biology, 2007. **177**(5): p. 857-870.

35. Sobotzik, J.-M., et al., *AnkyrinG is required to maintain axo-dendritic polarity in vivo.* Proceedings of the National Academy of Sciences of the United States of America, 2009. **106**(41): p. 17564-17569.

36. Kobayashi, T., et al., *A functional barrier to movement of lipids in polarized neurons.* Nature, 1992. **359**(6396): p. 647-650.

37. Winckler, B., P. Forscher, and I. Mellman, *A diffusion barrier maintains distribution of membrane proteins in polarized neurons.* Nature, 1999. **397**(6721): p. 698-701.

38. Leterrier, C. and B. Dargent, *No Pasaran! Role of the axon initial segment in the regulation of protein transport and the maintenance of axonal identity.* Semin Cell Dev Biol, 2014. **27**: p. 44-51.

39. Song, A.-h., et al., *A Selective Filter for Cytoplasmic Transport at the Axon Initial Segment.* Cell, 2009. **136**(6): p. 1148-1160.

40. Al-Bassam, S., et al., *Differential trafficking of transport vesicles contributes to the localization of dendritic proteins.* Cell Rep, 2012. **2**(1): p. 89-100.

41. Watanabe, K., et al., *Networks of Polarized Actin Filaments in the Axon Initial Segment Provide a Mechanism for Sorting Axonal and Dendritic Proteins.* Cell Reports, 2012. **2**(6): p. 1546-1553.

42. Arnold, D.B. and G. Gallo, *Structure meets function: actin filaments and myosin motors in the axon.* J Neurochem, 2014. **129**(2): p. 213-20.

43. Grubb, M.S. and J. Burrone, *Activity-dependent relocation of the axon initial segment fine-tunes neuronal excitability.* Nature, 2010. **465**(7301): p. 1070-1074.

44. Kuba, H., Y. Oichi, and H. Ohmori, *Presynaptic activity regulates Na+ channel distribution at the axon initial segment.* Nature, 2010. **465**(7301): p. 1075-1078.

45. Evans, M.D., et al., *Calcineurin signalling mediates activity-dependent relocation of the axon initial segment.* The Journal of neuroscience : the official journal of the Society for Neuroscience, 2013. **33**(16): p. 6950-6963.

46. Chand, A.N., et al., *A distinct subtype of dopaminergic interneuron displays inverted structural plasticity at the axon initial segment.* J Neurosci, 2015. **35**(4): p. 1573-90.

47. Normand, Elizabeth A. and Matthew N. Rasband, *Subcellular Patterning: Axonal Domains with Specialized Structure and Function.* Developmental Cell, 2015. **32**(4): p. 459-468.

48. Grubb, M.S., et al., *Short- and long-term plasticity at the axon initial segment.* J Neurosci, 2011. **31**(45): p. 16049-55.

49. Kaphzan, H., et al., *Alterations in intrinsic membrane properties and the axon initial segment in a mouse model of Angelman syndrome.* J Neurosci, 2011. **31**(48): p. 17637-48.

50. Ikezu, T. and H. Gendelman, *Neuroimmune Pharmacology*. 2008: Springer US.

51. Patestas, M.A. and L.P. Gartner, *Chapter 10 - Ascending Sensory Pathways*, in *A Textbook of Neuroanatomy*. 2013, Wiley.

52. Lallemend, F. and P. Ernfors, *Molecular interactions underlying the specification of sensory neurons.* Trends in Neurosciences, 2012. **35**(6): p. 373-381.

53. Andres, K.H., *Untersuchungen über den Feinbau von Spinalganglien.* Zeitschrift für Zellforschung und Mikroskopische Anatomie, 1961. **55**(1): p. 1-48.

54. Lee, K.H., et al., *Correlation of cell body size, axon size, and signal conduction velocity for individually labelled dorsal root ganglion cells in the cat.* J Comp Neurol, 1986. **243**(3): p. 335-46.

55. Lawson, S.N., *The postnatal development of large light and small dark neurons in mouse dorsal root ganglia: a statistical analysis of cell numbers and size.* J Neurocytol, 1979. **8**(3): p. 275-94.

56. Sommer, E.W., J. Kazimierczak, and B. Droz, *Neuronal subpopulations in the dorsal root ganglion of the mouse as characterized by combination of ultrastructural and cytochemical features.* Brain Res, 1985. **346**(2): p. 310-26.

57. Stanfield, C.L., *Principles of Human Physiology*. 2013, Pearson Education.

58. Caspary, T. and K.V. Anderson, *Patterning cell types in the dorsal spinal cord: what the mouse mutants say.* Nat Rev Neurosci, 2003. **4**(4): p. 289-297.

59. Harper, A.A. and S.N. Lawson, *Conduction velocity is related to morphological cell type in rat dorsal root ganglion neurones.* The Journal of Physiology, 1985. **359**: p. 31-46.

60. Perl, E.R., *Function of Dorsal Root Ganglion Neurons: An Overview*, in *Sensory Neurons: Diversity, Development, and Plasticity*, S.A. Scott, Editor. 1992, Oxford University Press. p. 3-23.

61. Gasser, H.S., *Effect of the method of leading on the recording of the nerve fiber spectrum.* J Gen Physiol, 1960. **43**: p. 927-40.

62. Lloyd, D.P. and H.T. Chang, *Afferent fibers in muscle nerves.* J Neurophysiol, 1948. **11**(3): p. 199-207.

63. Manzano, G.M., L.M.P. Giuliano, and J.A.M. Nóbrega, *A brief historical note on the classification of nerve fibers.* Arquivos de Neuro-Psiquiatria, 2008. **66**: p. 117-119.

64. Dubin, A.E. and A. Patapoutian, *Nociceptors: the sensors of the pain pathway.* The Journal of Clinical Investigation, 2010. **120**(11): p. 3760-3772.

65. Djouhri, L. and S.N. Lawson, *Abeta-fiber nociceptive primary afferent neurons: a review of incidence and properties in relation to other afferent A-fiber neurons in mammals.* Brain Res Brain Res Rev, 2004. **46**(2): p. 131-45.

66. Olson, W., et al., *The specification and wiring of mammalian cutaneous low-threshold mechanoreceptors.* Wiley Interdiscip Rev Dev Biol, 2016. **5**(3): p. 389-404.

67. Abraira, V.E. and D.D. Ginty, *The Sensory Neurons of Touch.* Neuron, 2013. **79**(4): p. 10.1016/j.neuron.2013.07.051.

68. Han, J., et al., *Assessing proprioception: A critical review of methods.* Journal of Sport and Health Science, 2016. **5**(1): p. 80-90.

69. Proske, U. and S.C. Gandevia, *The Proprioceptive Senses: Their Roles in Signaling Body Shape, Body Position and Movement, and Muscle Force.* Physiological Reviews, 2012. **92**(4): p. 1651-1697.

70. Schepers, R.J. and M. Ringkamp, *Thermoreceptors and thermosensitive afferents.* Neuroscience & Biobehavioral Reviews, 2009. **33**(3): p. 205-212.

71. Li, C.L., et al., *Somatosensory neuron types identified by high-coverage single-cell RNA-sequencing and functional heterogeneity.* Cell Res, 2016. **26**(1): p. 83-102.

72. Le Pichon, C.E. and A.T. Chesler, *The functional and anatomical dissection of somatosensory subpopulations using mouse genetics.* Frontiers in Neuroanatomy, 2014. **8**.

73. Usoskin, D., et al., *Unbiased classification of sensory neuron types by large-scale single-cell RNA sequencing.* Nat Neurosci, 2015. **18**(1): p. 145-53.

74. Ramón y Cajal, S., *Sur l'origin et les ramification des fibres nerveuses de la molle embryonnaire.* Anat Anz, 1890. **5**: p. 85-95.

75. Matsuda, S., et al., *Morphological transformation of sensory ganglion neurons and satellite cells.* Kaibogaku Zasshi, 2000. **73**(6): p. 603-13.

76. His, W., *Zur Geschichte des menschlichen Rückenmarkes und der Nervenwurzeln*, in *Abhandlungen der mathematisch-physischen classe der königlich sächsischen gesellschaft der wissenschaften*. 1886. p. 479-513.

77. Ramón y Cajal, S., *Asociación del método del nitrato de plata con el embrionario para el estudio de los focos motores y sensitivos.* Trab. Lab. Invest. Bio. Univ. Madrid, 1904. **3**: p. 65-96.

78. Matsuda, S., et al., *Dorsal root ganglion neuron development in chick and rat.* Anat Embryol (Berl), 1996. **193**(5): p. 475-80.

79. Matsuda, S. and Y. Uehara, *Prenatal development of the rat dorsal root ganglia. A scanning electron-microscopic study.* Cell Tissue Res, 1984. **235**(1): p. 13-8.

80. Tennyson, V.M., *Electron microscopic study of the developing neuroblast of the dorsal root ganglion of the rabbit embryo.* J Comp Neurol, 1965. **124**(3): p. 267-317.

81. Barber, R.P. and J.E. Vaughn, *Differentiation of dorsal root ganglion cells with processes in their synaptic target zone of embryonic mouse spinal cord: a retrograde tracer study.* J Neurocytol, 1986. **15**(2): p. 207-18.

82. Riederer, B.M. and I. Barakat-Walter, *Differential distribution of two microtubule-associated proteins, MAP2 and MAP5, during chick dorsal root ganglion development in situ and in culture.* Brain Res Dev Brain Res, 1992. **68**(1): p. 111-23.

83. Rámon y Cajal, S., *Histologie du système nerveux de l'homme et des Vertèbres*, ed. Maloine. Vol. 1. 1955, Paris: Maloine.

84. Takahashi, K. and T. Ninomiya, *Morphological changes of dorsal root ganglion cells in the process-forming period.* Prog Neurobiol, 1987. **29**(4): p. 393-410.

85. Ribeiro, A., et al., *Substrate Three-Dimensionality Induces Elemental Morphological Transformation of Sensory Neurons on a Physiologic Timescale.* Tissue Engineering. Part A, 2012. **18**(1-2): p. 93-102.

86. De Koninck, P., S. Carbonetto, and E. Cooper, *NGF induces neonatal rat sensory neurons to extend dendrites in culture after removal of satellite cells.* J Neurosci, 1993. **13**(2): p. 577-85.

87. Mudge, A.W., *Schwann cells induce morphological transformation of sensory neurones in vitro.* Nature, 1984. **309**(5966): p. 367-369.

88. Khan, A.A., M. Naushad, and A. Dilkash, *Morphological heterogeneity in the cervical dorsal root ganglion neurons of mice.* Curr Neurobiol, 2011. **2**(2): p. 125-128.

89. Pannese, E., *The structure of the perineuronal sheath of satellite glial cells (SGCs) in sensory ganglia.* Neuron Glia Biol, 2010. **6**(1): p. 3-10.

90. Hess, A., *The fine structure of young and old spinal ganglia.* The Anatomical Record, 1955. **123**(4): p. 399-423.

91. Matsuda, S., et al., *Perikaryal projections of developing spinal ganglion neurons in the chick demonstrated by scanning electron microscopy.* Anat Embryol (Berl), 1997. **195**(2): p. 137-46.

92. Pannese, E., et al., *Perikaryal projections of spinal ganglion neurons: quantitative differences between membrane domains in contact with different microenvironments.* Journal of Anatomy, 1994. **185**(Pt 3): p. 497-502.

93. Pannese, E., et al., *The perikaryal surface of spinal ganglion neurons: differences between domains in contact with satellite cells and in contact with the extracellular matrix.* Anat Embryol (Berl), 1999. **199**(3): p. 199-206.

94. Pannese, E., et al., *Age-related decrease in the overall extent of perikaryal projections in rabbit spinal ganglion neurons.* Neuroscience Letters, 1998. **254**(3): p. 177-179.

95. Ramón y Cajal, S., *Textura del sistema nervioso del hombre y los vertebrados*, ed. Moya. 1899, Madrid.

96. Matsuda, S., et al., *Phylogenetic investigation of Dogiel's pericellular nests and Cajal's initial glomeruli in the dorsal root ganglion.* The Journal of Comparative Neurology, 2005. **491**(3): p. 234-245.

97. Kayahara, T., T. Takimoto, and S. Sakashita, *Synaptic junctions in the cat spinal ganglion.* Brain Research, 1981. **216**(2): p. 277-290.

98. Chung, K., Y.W. Yoon, and J.M. Chung, *Sprouting sympathetic fibers form synaptic varicosities in the dorsal root ganglion of the rat with neuropathic injury.* Brain Research, 1997. **751**(2): p. 275-280.

99. Ramer, M.S. and M.A. Bisby, *Normal and injury-induced sympathetic innervation of rat dorsal root ganglia increases with age.* The Journal of Comparative Neurology, 1998. **394**(1): p. 38-47.

100. McLachlan, E.M., et al., *Peripheral nerve injury triggers noradrenergic sprouting within dorsal root ganglia.* Nature, 1993. **363**(6429): p. 543-6.

101. Devor, M., W. Janig, and M. Michaelis, *Modulation of activity in dorsal root ganglion neurons by sympathetic activation in nerve-injured rats.* J Neurophysiol, 1994. **71**(1): p. 38-47.

102. Hofstetter, C.P., J.P. Card, and L. Olson, *A spinal cord pathway connecting primary afferents to the segmental sympathetic outflow system.* Experimental Neurology, 2005. **194**(1): p. 128-138.

103. Hsieh, S.T., et al., *Regional modulation of neurofilament organization by myelination in normal axons.* J Neurosci, 1994. **14**(11 Pt 1): p. 6392-401.

104. Hongchien, H., *Axonal bifurcation in the dorsal root ganglion of the cat: a light and electron microscopic study.* J Comp Neurol, 1970. **140**(2): p. 227-40.

105. Matsuda, S. and Y. Uehara, *Cytoarchitecture of the rat dorsal root ganglia as revealed by scanning electron microscopy.* J Electron Microsc (Tokyo), 1981. **30**(2): p. 136-40.

106. Spencer, P.S., C.S. Raine, and H. Wisniewski, *Axon diameter and myelin thickness. Unusual relationships in dorsal root ganglia.* Anat Rec, 1973. **176**(2): p. 225-43.

107. Zenker, W. and E. Högl, *The prebifurcation section of the axon of the rat spinal ganglion cell.* Cell and tissue research, 1976. **165**(3): p. 345-363.

108. Matsumoto, E. and J. Rosenbluth, *Plasma membrane structure at the axon hillock, initial segment and cell body of frog dorsal root ganglion cells.* J Neurocytol, 1985. **14**(5): p. 731-47.

109. Bird, M.M. and A.R. Lieberman, *Microtubule fascicles in the stem processes of cultured sensory ganglion cells.* Cell Tissue Res, 1976. **169**(1): p. 41-7.

110. Zelená, J., *Ribosomes in myelinated axons of dorsal root ganglia.* Z Zellforsch Mikrosk Anat, 1972. **124**(2): p. 217-29.

111. Nakazawa, E. and H. Ishikawa, *Occurrence of fasciculated microtubules at nodes of Ranvier in rat spinal roots.* J Neurocytol, 1995. **24**(5): p. 399-407.

112. Chan-Palay, V., *The tripartite structure of the undercoat in initial segments of Purkinje cell axons.* Z Anat Entwicklungsgesch, 1972. **139**(1): p. 1-10.

113. Devor, M., P.D. Wall, and S.B. McMahon, *Dichotomizing somatic nerve fibers exist in rats but they are rare.* Neuroscience Letters, 1984. **49**(1–2): p. 187-192.

114. Suh, Y.S., K. Chung, and R.E. Coggeshall, *A study of axonal diameters and areas in lumbosacral roots and nerves in the rat.* J Comp Neurol, 1984. **222**(4): p. 473-81.

115. Ochs, S., et al., *Routing of transported materials in the dorsal root and nerve fiber branches of the dorsal root ganglion.* J Neurobiol, 1978. **9**(6): p. 465-81.

116. Pannese, E., et al., *An electron microscope study of quantitative relationships between axon and Schwann cell sheath in myelinated fibres of peripheral nerves.* Anat Embryol (Berl), 1987. **175**(4): p. 423-30.

117. Pannese, E., et al., *Quantitative relationships between axoplasm and Schwann cell sheath in unmyelinated nerve fibres. An electron microscope study.* Journal of Anatomy, 1988. **159**: p. 49-56.

118. Fadic, R., J. Vergara, and J. Alvarez, *Microtubules and caliber of central and peripheral processes of sensory axons.* J Comp Neurol, 1985. **236**(2): p. 258-64.

119. Pannese, E., et al., *A quantitative study of microtubules in motor and sensory axons.* Acta Anat (Basel), 1984. **118**(4): p. 193-200.

120. Smith, R.S., *Microtubule and neurofilament densities in amphibian spinal root nerve fibers: relationship to axoplasmic transport.* Can J Physiol Pharmacol, 1973. **51**(11): p. 798-806.

121. Tsukita, S. and H. Ishikawa, *Three-dimensional distribution of smooth endoplasmic reticulum in myelinated axons.* J Electron Microsc (Tokyo), 1976. **25**(3): p. 141-9.

122. Berthold, C.H., et al., *Axoplasmic organelles at nodes of Ranvier. I. Occurrence and distribution in large myelinated spinal root axons of the adult cat.* J Neurocytol, 1993. **22**(11): p. 925-40.

123. Pannese, E. and M. Ledda, *Ribosomes in myelinated axons of the rabbit spinal ganglion neurons.* J Submicrosc Cytol Pathol, 1991. **23**(1): p. 33-8.

124. Rosenbluth, J., *Multiple functions of the paranodal junction of myelinated nerve fibers.* J Neurosci Res, 2009. **87**(15): p. 3250-8.

125. Berthold, C.-H. and M. Rydmark, *Electron microscopic serial section analysis of nodes of Ranvier in lumbosacral spinal roots of the cat: ultrastructural organization of nodal compartments in fibres of different sizes.* Journal of Neurocytology, 1983. **12**(3): p. 475-505.

126. Du, X., et al., *Control of somatic membrane potential in nociceptive neurons and its implications for peripheral nociceptive transmission.* Pain, 2014. **155**(11): p. 2306-2322.

127. Loeb, G.E., *Decreased conduction velocity in the proximal projections of myelinated dorsal root ganglion cells in the cat.* Brain Research, 1976. **103**(2): p. 381-385.

128. Czéh, G., N. Kudo, and M. Kuno, *Membrane properties and conduction velocity in sensory neurones following central or peripheral axotomy.* The Journal of Physiology, 1977. **270**(1): p. 165-180.

129. Ochs, S., *Rate of fast axoplasmic transport in mammalian nerve fibres.* The Journal of Physiology, 1972. **227**(3): p. 627-645.

130. Komiya, Y. and M. Kurokawa, *Asymmetry of protein transport in two branches of bifurcating axons.* Brain Research, 1978. **139**(2): p. 354-358.

131. Wujek, J.R. and R.J. Lasek, *Correlation of axonal regeneration and slow component B in two branches of a single axon.* J Neurosci, 1983. **3**(2): p. 243-51.

132. Hoffman, P.N., *A conditioning lesion induces changes in gene expression and axonal transport that enhance regeneration by increasing the intrinsic growth state of axons.* Experimental Neurology, 2010. **223**(1): p. 11-18.

133. Namgung, U., *The role of Schwann cell-axon interaction in peripheral nerve regeneration.* Cells Tissues Organs, 2014. **200**(1): p. 6-12.

134. Carmel, P.W. and B.M. Stein, *Cell changes in sensory ganglia following proximal and distal nerve section in the monkey.* J Comp Neurol, 1969. **135**(2): p. 145-66.

135. Zhang, X. and V. Bennett, *Restriction of 480/270-kD Ankyrin (G) to Axon Proximal Segments Requires Multiple Ankyrin (G)-specific Domains.* The Journal of Cell Biology, 1998. **142**(6): p. 1571-1581.

136. Lambert, S., J.Q. Davis, and V. Bennett, *Morphogenesis of the node of Ranvier: co-clusters of ankyrin and ankyrin-binding integral proteins define early developmental intermediates.* J Neurosci, 1997. **17**(18): p. 7025-36.

137. Eshed, Y., et al., *Gliomedin Mediates Schwann Cell-Axon Interaction and the Molecular Assembly of the Nodes of Ranvier.* Neuron, 2005. **47**(2): p. 215-229.

138. Ho, T.S.-Y., et al., *A hierarchy of ankyrin-spectrin complexes clusters sodium channels at nodes of Ranvier.* Nat Neurosci, 2014. **17**(12): p. 1664-1672.

139. Beaudoin, G.M.J., et al., *Culturing pyramidal neurons from the early postnatal mouse hippocampus and cortex.* Nat. Protocols, 2012. **7**(9): p. 1741-1754.

140. Evans, M.D., et al., *Rapid Modulation of Axon Initial Segment Length Influences Repetitive Spike Firing.* Cell Rep, 2015. **13**(6): p. 1233-45.

141. Feng, G., et al., *Imaging neuronal subsets in transgenic mice expressing multiple spectral variants of GFP.* Neuron, 2000. **28**(1): p. 41-51.

142. Bishop, D., et al., *Near-infrared branding efficiently correlates light and electron microscopy.* Nat Methods, 2011. **8**(7): p. 568-70.

143. Micholt, L., et al., *Substrate Topography Determines Neuronal Polarization and Growth In Vitro.* PLoS ONE, 2013. **8**(6): p. e66170.